Investigation of hand and arm synergies based on electromyographic data

A Thesis

submitted to
Indian Institute of Science Education and Research Pune
in partial fulfillment of the requirements for the
BS-MS Dual Degree Programme

by

Prerana Kumar

Indian Institute of Science Education and Research Pune
Dr. Homi Bhabha Road,
Pashan, Pune 411008, INDIA.

May, 2020

Supervisor: Prof. Martin Giese

Certificate

This is to certify that this dissertation entitled “Investigation of hand and arm synergies based on electromyographic data" towards the partial fulfilment of the BS-MS dual degree programme at the Indian Institute of Science Education and Research, Pune represents study/work carried out by Prerana Kumar at the University of Tübingen, Germany under the supervision of Prof. Martin Giese, Professor, Department of Cognitive Neurology , during the academic year 2019-2020.

Prerana Kumar

Dr. Collins Assisi

Prof. Martin Giese

Committee:
Prof. Martin Giese
Dr. Collins Assisi

This thesis is dedicated to Poorna, my elder sister.

Declaration

I hereby declare that the matter embodied in the report entitled “Investigation of hand and arm synergies based on electromyographic data" are the results of the work carried out by me at the Department of Cognitive Neurology, University of Tübingen, Germany under the supervision of Prof. Martin Giese and the same has not been submitted elsewhere for any other degree.

Prerana Kumar

Dr. Collins Assisi

Prof. Martin Giese

Acknowledgments

I would like to express my deep gratitude to my supervisor, Prof. Martin Giese, for being a wonderful and approachable mentor from whom I gained invaluable knowledge during the course of my master's thesis project. I am grateful to him for giving me the opportunity to do my master's thesis project in his lab and look forward to our future work together.

I am thankful to my TAC expert, Dr. Collins Assisi, for his encouragement and suggestions. His relevant questions during my mid-year presentation made me think more about, and better understand, certain aspects of my project. Dr. Assisi's thought-provoking lectures in my undergraduate Systems Biology course initiated my interested in quantitative biology.

I thank Dr. Leonardo Gizzi for his valuable guidance regarding our experiments and the EMG analysis. I would like to thank Jesse St. Amand, whose project I worked on, for his many helpful suggestions and our discussions regarding different aspects of the project, which helped me gain greater clarity on many topics. I am very grateful to Dr. Albert Mukovskiy for helping me with the analysis, patiently answering my many questions and introducing me to many useful analysis techniques.

I would also like to thank Dr. Alia Benali for taking the time out of her busy schedule to help us procure the apparatus for our experiments. For their valuable help, I am grateful to Dominic Hillerkuss, Alessandro Salatiello, Michael Stettler and Mirjana Angelovska. I enjoyed being part of a fantastic lab environment thanks to all the lab members at Compsens.

I wish to thank all my friends, especially Palash Singh and Shruti Jose, for their support and encouragement during the past year.

I am fortunate to be part of an open-minded and supportive family. They have always encouraged me to follow my dreams, and for that, I am immensely grateful.

Abstract

Natural upper limb motion is characterized by efficient coordination between the hand and the arm. Based on underlying coordination patterns, high-density (HD) surface electromyographic (sEMG) signals from the upper limb can be used along with regular sEMG signals to predict hand kinematics. Accurate predictions of hand kinematics from EMG signals are integral for the development of high-performance robotic finger prostheses or increasing the reliability of existing ones. To obtain a better understanding of the mapping between regular and HD-sEMG signals and the kinematics of the upper limb, we created and optimized a novel experimental setup, using which, two pilot experiments were performed on a healthy subject. In these experiments, we measured motion capture data as well as regular and HD-sEMG signals from the subject's upper limb, during directional point-to-point grasping of target blocks located in a fixed plane. We used the Fourier-based Anechoic Demixing Algorithm (FADA) to identify and characterize the spatiotemporal synergies present in the sEMG data. We found the 1:1 mapping between the arm and hand synergies, and the synergies extracted from all the muscles combined. The similarity between the hand synergies and the corresponding synergies from all the muscles combined was much higher than that between the arm synergies and the latter. 3 spatiotemporal synergies were sufficient to successfully reconstruct the 9 directional grasping movements.The reconstructions obtained explained more than 80 % of the variation in the data.

List of Figures

3.1 Target blocks numbering scheme 14
3.2 Experimental setup 16
3.3 Data recording in progress 17
3.4 Vertical framework setup 22
3.5 Horizontal framework setup 22
3.6 Correlated HD-array spike trains 28
3.7 Spatial clustering 30
3.8 Silhouette plot HD-array 1 31
3.9 Silhouette plot HD-array 2 31
3.10 Silhouette plot HD-array 3 31

4.1 EMG data of arm channels (experiment 1) 37
4.2 ANOVA results (5 trials) 38
4.3 ANOVA results (3 trials) 39
4.4 EMG data from arm channels (experiment 2) 40
4.5 Number of synergies versus R^2 for arm channel synergies 41
4.6 Number of synergies versus R^2 for hand channel synergies 41
4.7 Number of synergies versus R^2 for combined-channel synergies 41
4.8 Arm muscle synergies 42
4.9 Hand muscle synergies 43
4.10 Combined-channel synergies 44
4.11 Reconstruction of arm data from arm synergies 45
4.12 Reconstruction of hand data from hand synergies 46
4.13 Reconstruction of arm channels from combined-channel synergies 47
4.14 Reconstruction of hand channels from combined-channel synergies 48
4.15 Similarity table of the arm synergies and combined-channel synergies 49
4.16 Similarity table of the hand synergies and combined-channel synergies 49

Thesis Roadmap

This master's thesis consists of 5 chapters:

- Chapter 1 - Introduction: Provides background information, lays out the objectives of this project and illustrates the context in which the research question being addressed has been established.
- Chapter 2 - The Fourier-Based Anechoic Demixing Algorithm (FADA): A significant part of this project is based on the analysis of muscle synergies from EMG data. This chapter explains in detail the main algorithm used to find these muscle synergies.
- Chapter 3 - Materials and Methods: Provides a description of the materials and methods used for the experiments conducted and for the offline analysis of the data.
- Chapter 4 - Results: Contains a record of all the results obtained including graphs, figures and tables.
- Chapter 5 - Discussion: Provides a brief summary and interpretation of the results, and possible future analysis of the data.

Contents

Abstract vi

1 Introduction 1
- 1.1 Synergy-based view of motor control 1
- 1.2 Neural interfaces for upper-limb motor impairment caused by stroke 2
- 1.3 Pillars of muscle synergy studies: EMG and Motion Capture Data 3
- 1.4 Objectives 5

2 The Fourier-Based Anechoic Demixing Algorithm (FADA) algorithm 7
- 2.1 Spatiotemporal primitives generative model 7
- 2.2 Anechoic mixture model (Unifying model) 8
- 2.3 Identification of spatiotemporal synergies using the anechoic demixing algorithm 10
- 2.4 Variance explained measure for synergies 11

3 Materials and Methods 13
- 3.1 Pilot Experiment 1 13
- 3.2 Additional data collected 19
- 3.3 Observations 19
- 3.4 Pilot Experiment 2 20
- 3.5 EMG signal processing and analysis 25

4 Results 36
- 4.1 EMG Data (Pilot Experiment 1) 36
- 4.2 EMG data (Pilot experiment 2) 39
- 4.3 Plots of explained variance (R^2) vs number of synergies 41
- 4.4 Synergies extracted from the 3 groups of data 42
- 4.5 Data reconstruction from muscle synergies 45
- 4.6 Synergy similarity analysis results 49
- 4.7 Reconstruction of combined channel data using 1 synergy at a time 49

5 Discussion 51

Chapter 1

Introduction

1.1 Synergy-based view of motor control

How does the musculoskeletal system generate the large number of muscular patterns required to facilitate the different types of behaviours? Muscle pattern generation for different physical tasks can be considered as a very complex control problem, because it involves the mapping of a potentially infinite number of muscle patterns onto a set of potentially infinite physical tasks or behaviours (d'Avella et al., 2003). Previous research has pointed to the existence of a limited set of generators that are used by the Central Nervous System (CNS) for the generation of the different patterns required for the execution of different motor tasks (Singh et al., 2018). Such an organization is advantageous to the CNS because it reduces the dimensionality of the problem and allows for the sharing of neural circuitry across the different tasks. These generators are called muscle synergies or movement primitives (d'Avella et al., 2003, Flash et al., 2005, d'Avella et al., 2006, Singh et al., 2018, Scano et al., 2019). According to motor control literature, the definition of a muscle synergy or movement primitive is the coordinated recruitment of a particular set of muscles which have specific activation wave-forms. Each muscle is assumed to be acted upon by a number of synergies, and its net activation is the sum of the effects of each of the synergies (Flash et al., 2005).

An important feature of this particular view of motor control is the ability to generate multiple types of movements from a limited number of synergies by transforming and operating on them appropriately. Each synergy produces a torque about a joint or a force in a particular direction (Flash et al., 2005). The simple movements generated by the synergies are in turn combined appropriately to form more complex actions or behaviours.

An implicit assumption of this view is that since synergies are coded for at the level of neurons, a unique set of synergies can be used to generate a variety of movements or, at least, a specific set can explain the different movement variations corresponding to tasks that require similar motor commands for their execution. Thus, according to this view, the same set of synergies may underlie different variations of the same task (for example, grasping movements in different directions), but different tasks associated with dissimilar motor commands may require additional or different synergies (D'avella et al., 2003).

The representation of high-dimensional signals using limited muscle synergies has attracted considerable interest in the field of robotics research. Using a small set of synergies to represent high-dimensional data can considerably reduce the complexity and high-dimensionality which are commonly associated with robot control problems. Thus, multiple robotics studies (Alessandro et al., 2013, Lunardini et al., 2016, Cimolato et al., 2016) have attempted to thoroughly characterize muscle synergies and studied their mathematical extraction and potential to be used in robotic imitations of human movements.

1.2 Neural interfaces for upper-limb motor impairment caused by stroke

Strokes are the second leading cause of death worldwide, and their incidence has more than doubled in developing countries, such as India (Johnson et al., 2016). According to the WHO, more than 15 million people are affected by strokes worldwide, annually. A stroke is the sudden death of some brain cells as a result of lack of access to oxygen caused by the blockage or rupture of an artery in the brain (Johnson et al., 2016). The effects of a stroke are dependent on the location and extent of damage. One of the most common consequences of a stroke is the hemiparesis of the contralateral upper limb (Hatem et al., 2016). This means that the upper limb on the side of the body opposite to the injured hemisphere of the brain exhibits weakness or impaired motor control, typically at the extremities. These impairments may affect the individual's ability to perform common activities such as reaching, grasping or picking up objects. Most affected muscles can only produce weak or residual electromyographic (EMG activity), if any, which is insufficient to elicit a proper motor response. The fact that every year, there are a large number of people who suffer strokes and require biorobotic devices to facilitate lost up-

per limb movement, makes a strong case for the establishment of concentrated research efforts to better understand upper limb motor control.

Efficient coordination between the hand and the arm is essential for natural upper limb motion (Legrande et al., 2018). A thorough understanding of underlying coordination patterns involved is required for the construction of efficient robotic devices such as MI (myoelectric interface) controlled arm ortheses or exoskeletons. In patients who have undergone a hand amputation, the remaining arm muscles may still generate weak EMG signals. These signals can potentially be supplemented or strengthened by a myoelectric interface (MI) that interprets them and sends control commands to a body actuator (Sarasola-Sanz et al., 2015). Such a device, if attached to the impaired limb, can subsequently reproduce the decoded movement. An important requirement for the construction of such devices is a thorough understanding of the mapping between the EMG signals generated in the arm and the kinematics of the hand and fingers. Another important requirement is the ability to predict hand and finger kinematics from the kinematics of the arm. An intelligent hand orthesis could be designed to control hand movement based on EMG input from the arm and lower hand muscles, in coordination with arm movement, with the intention of the user encoded as an additional input.

1.3 Pillars of muscle synergy studies: EMG and Motion Capture Data

To study the underlying coordination patterns of movements, two kinds of data are often measured - electromyographic (EMG) data and motion capture data.

1.3.1 EMG data

Electrical signals are conducted by muscle tissues in a manner similar to that present in axons. A motor neuron and all the skeletal muscle fibers that it innervates are collectively called a motor unit (A. Winter, 1990). When a motor unit is recruited, the electrical signals produced in the muscle fibers in response, constitute a motor unit action potential. A surface electrode placed above a muscle records the algebraic sum of all the motor unit action potentials being conducted along muscle fibers at that time (Rodriguez-Carreno et al., 2012).

Electromyography is a technique used to measure the response or electrical activity of skeletal muscles that occurs as a consequence of their stimulation by nerves (Raez et al., 2006). The instrument used to produce these readings is called an electromyograph, and the data record obtained is termed as an electromyogram. An electromyograph measures the change in potential caused by the activation of a muscle. A muscle tissue usually shows no activity during periods of rest, and the magnitude of the EMG readings obtained is directly proportional to the level of activation or force exerted by the muscle whose activity is being recorded (Kuriki et al., 2012). The more forceful the muscle contraction, the greater the number of muscle fibres activated, resulting in a higher net activation of the muscle.

Motor units far away from the electrode site will cause a smaller motor unit action potential than those of similar size near the electrode (Winter et al., 1994). When electrodes detect and record signals produced by the muscle of interest as well as those produced by other muscles, this is known as cross-talk. A commonly experienced issue when taking EMG readings across multiple trials is the non-stationarity of EMG signals across the different trials (Nazmi et al., 2016).

There exist two types of EMG data - surface EMG (sEMG) data and intramuscular EMG data (Jamal, 2012). To obtain intramuscular EMG recordings, narrow needles (electrodes) are inserted through the skin directly into the muscle of interest and its activation is directly measured. This method is advantageous over sEMG because the readings obtained are more accurate. However, one drawback of this method is that due to its invasive nature, it can only be performed on human subjects by licensed professionals. Additionally, the data recorded lacks spatial information (Marateb et al., 2016). Thus, in our experiments, we recorded sEMG signals from the arm muscles.

sEMG readings are obtained from muscles by measuring the changes in electrical potential from a patch of skin directly above the muscle of interest (Chowdhury et al.,2013). The assumption is that the readings measured from an area of skin are largely produced by the activity of the muscle closest to it. However, a smaller part of the readings may be made up of the action potentials of other more distal muscles, affecting their accuracy.

Another drawback regarding sEMG measurements is the fact that the signals produced by the muscles need to travel through layers of subcutaneous tissue before they reach the surface of the skin and are measured. This results in attenuation and alteration of signals before they are measured by surface electrodes, lowering the accuracy of the readings obtained (Turker, 1993). Additionally, the features of sEMG signal are depen-

dent on the internal structure specific to the subject being measured, such as the skin formation of the individual, the velocity of blood flow near the area being measured, the temperature of the skin at the site of measurement, the structure of the underlying tissue and the particular site being measured.

High density-surface EMG (HD-sEMG) is also a non-invasive method used to measure the electrical activity of muscles, the difference from regular sEMG being the use of numerous (more than two) electrodes in the form of densely packed arrays to measure signals from a small, well-defined region of the skin (Drost et al., 2006). Apart from providing information regarding the temporal activity of the muscles being recorded, HD-sEMG also allows for the recording of spatial EMG activity, increasing the scope of muscle characteristics that can be recorded. This technology increases the feasibility of the evaluation of single motor unit (MU) features or the measurement of muscle fiber conduction velocities (MFCV)(Drost et al., 2006).

1.3.2 Kinematics data

Motion capture is the process of recording the movements carried out by the human or animal being studied (Filho, 2005). Using this technique, retroreflective markers are placed on the body of the subject, and the movement is tracked and recorded by infrared cameras. One drawback of this technique is the occlusion of markers by objects that may hide them from the view of the cameras while the subject performs the action. Motion capture systems help in understanding the dynamics of movements at the level of the different joint segments, providing useful insights into the overall bio-mechanics of body movement. Precise kinematics data is crucial for the advancement of prosthesis research (Legrande et al., 2018). The light and non-invasive nature of the reflective markers makes this a convenient method of recording the dynamics of movements.

1.4 Objectives

The aim of this master's thesis project was to investigate the hand and arm synergies underlying a task which involved grasping well-defined targets at fixed positions on a planar frame. Investigating the nature of the muscle synergies involved in hand and arm coordination in this task was a step leading towards exploring the prediction of hand kinematics from sEMG signals. This project was a part of a larger effort to build an intelligent non-

invasive exoskeleton device to potentially rehabilitate and supplement lost movement in patients suffering from partial or total paralysis of the arm.

The EMG data analyzed in this project were recorded during two pilot experiments. These experiments were carried out in order to develop and optimize a controlled experimental setup for recording regular and HD-sEMG signals from the hand and arm, as well as motion capture signals. More specifically, the objectives of the two experiments were the following:

1.4.1 Pilot Experiment 1

The chief purpose of this study was to obtain some preliminary EMG and motion capture data to use as a basis for understanding the underlying data structure and the mapping between them. This dataset was intended to be used for the development of a robust data processing and analysis pipeline. The experiment was carried out as a pilot study on a single subject in order to test our experimental setup and protocol, and the quality of the data was assessed after some preliminary data processing. The aim was to modify the experimental protocol appropriately for future experiments based on the data quality, feedback from the subject and our experience conducting the experiment.

1.4.2 Pilot Experiment 2

The main aim of the second pilot experiment was to obtain better quality EMG and motion capture recordings by modifying the experiment design based on our analysis of the data previously obtained. Another goal was to obtain a more expansive dataset by incorporating two different experimental frame setups (vertical and horizontal), two different grasp types (precision and power grip) and two different types of reaching movements (with supination and without supination) to record six different grasp types, which are listed in the Materials and Methods section.

Chapter 2

The Fourier-Based Anechoic Demixing Algorithm (FADA) algorithm

The process of extracting a set of source signals from a mixture of signals without having much information regarding the number of source signals or the process used to mix them is known as blind source separation. It is often used in the digital processing of signals, such as EMG signals, with the objective being to extract and separate the original components of the signal from the mixed signal. The Fourier-based Anechoic Demixing Algorithm (Chiovetto et al., 2016), which was used in this project to identify muscle synergies, is a unifying algorithm which performs source (synergy) separation by means of anechoic demixing.

2.1 Spatiotemporal primitives generative model

This generative model is used to model EMG components that are both space and time invariant. The model permits temporal shifts (delays) between the different synergies. The following equation represents the spatiotemporal generative model, where $\mathbf{x}^l(t)$ is representative of the time-dependent column vector of the degree of freedom (EMG channel):

$$\mathbf{x}^l(t) = \sum_{p=1}^{P} c_p^l \cdot \mathbf{w}_p(t - \tau_p^l) + \text{residuals} \tag{2.1}$$

While the synergies denoted by $\mathbf{w}_p(t)$ are assumed to be invariant across trials, the mixing weights c_p^l and delays τ_p^l change across the different trials.

2.2 Anechoic mixture model (Unifying model)

Models of this type are utilized in acoustics for modeling mixtures of sources in rooms that are free of reverberation. In this model, U acoustic source functions $f_u(t)$ are linearly superposed by time-shifting them with delays denoted by τ_{ru}, along with the application of appropriate mixing weights a_{ru}, to form a set of R recorded acoustic signals $y_r(t)$. This model also accounts for the fact that the signals produced by sources are received with different time-delays and strengths (amplitudes), which are dependent upon the distance between the receiver and the origins of the signals. The form of the generative model is as denoted below:

$$y_r(t) = \sum_{u=1}^{U} a_{ru} \cdot f_u(t - \tau_{ru}) + \text{residuals} \tag{2.2}$$

The anechoic demixing problem that we were trying to solve was the over-determined case, where the signals (one per channel) outnumbered the sources. This case of the problem is extremely relevant for dimensionality reduction applications, but has not been addressed as often as the under-determined case.

A considerable number of parameters have to be identified when standard algorithms are used for blind source separation. Let T, M, U and L represent the total number of time samples, degrees of freedom, sources and trials. Given the model represented by Eq. (2.2), for the representation of all sources $f_u(t)$, $T \cdot U$ parameters must be identified. For every trial L, $M \cdot U$ weights and delays need to be identified. Taking the entire dataset into consideration, this results in a total of $(T + 2M \cdot L) \cdot U$ parameters which must be identified, where $T >> M, U, L$.

The unifying algorithm, which can be used to identify the parameters in the unconstrained model represented by Eq. (2.2), makes use of the fact that biological signals in motor control are typically smooth. This enables a significant reduction in the complexity of the anechoic demixing problem and facilitates the development of a more robust approach to the problem. Since EMG signals are very smooth, they can be well represented by smooth source signals. Smoothing priors are used to represent the source signals, which increases the stability of the source separation problem. Another feature of the algorithm is the use of truncated Fourier expansions to represent the smooth sources. $K(<< T)$ Fourier coefficients can be used to reasonably approximate each of the sources. As a result, the number of parameters that need to be identified reduces to $(K + 2M \cdot L) \cdot U$, significantly decreasing the computational costs associated with pa-

rameter estimation and increasing the robustness of the algorithm. Another assumption made is that the sources and the signals are band-limited, justifying their representation by truncated Fourier expansions. They can be represented as follows:

$$\begin{aligned} y_r(t) &= \sum_{k=-K}^{K} c_{rk}\, e^{\frac{2\pi ikt}{T_s}} \\ f_u(t-\tau_{ru}) &\cong \sum_{k=-K}^{K} \nu_{uk}\, e^{-ik\tau_{ru}}\, e^{\frac{2\pi ikt}{T_s}} \end{aligned} \tag{2.3}$$

The source decomposition algorithm ensures that the different source functions are not correlated. Thus it is implied that $E\{f_u(t) \cdot f_{u'}(t')\} = 0$ for $u \neq u'$ and any pair $t \neq t'$. This implies $E\{\nu_{uk} \cdot \nu_{u'k'}\} = 0$ for $u \neq u'$ and any pair $k \neq k'$ for the Fourier coefficients involved. On combining equations Eq. (2.2) and Eq. (2.3) we get:

$$c_{rk} = \sum_{u=1}^{U} a_{ru} \cdot \nu_{uk}\, e^{-ik\tau_{ru}} \tag{2.4}$$

from this equation, with $E\{\nu_{uk} \cdot \nu^*{}_{u'k'}\} = E\{|\nu_{uk}|^2\} \cdot \delta_{uu'}$ follows:

$$|c_{rk}|^2 = \sum_{u=1}^{U} |a_{ru}|^2 |\nu_{uk}|^2 \tag{2.5}$$

The estimated parameters are randomly initialized, after which the steps listed below are carried out until the solutions converge:

1. The absolute values of the coefficients denoted by c_{rk} are computed and used to solve the following equation:

$$|c_{rk}|^2 = \sum_{u=1}^{U} |a_{ru}|^2 |\nu_{uk}|^2 \tag{2.6}$$

   where $r = 0, 1, 2, \ldots, R$ and $k = 0, 1, , \ldots, K$. Non-negative independent component analysis (ICA) is used by the algorithm to solve the above equation. ICA is a computational technique used to extract the additive subcomponents from a multivariate signal. The assumptions in this method are that the subcomponents are statistically independent, non-Gaussian signals. Non-negative ICA imposes a non-negative constraint on the sources.

2. All the pairs are initialized and the following steps are carried out:

   (a) The phases of the Fourier coefficients of the sources given by $\varphi_{\mu_{uk}} = angle(\nu_{uk}) = arctan(Im(\nu_{uk})/Re(\nu_{uk}))$ are updated by solving the following non-linear least square problem:

   $$\min_{\mathbf{\Phi}} ||\mathbf{C} - \mathbf{Z}(\mathbf{\Phi})||_F^2 \tag{2.7}$$

   where $(\mathbf{C})_{rk} = c_{rk}, (\mathbf{Z})_{rk} = \sum_{u=1}^{U} a_{ru}\, e^{-ik\tau_{uk}} |\nu_{uk}| e^{i\varphi\nu_{uk}}$ and represents the Frobenius norm, which is the square root of the sum of the absolute squares of all the elements of the matrix.

   (b) The separated source functions $f_u(t)$ are kept constant, and for each signal $y_r(t)$ by minimizing the following cost functions

   $$arg\ min_{\mathbf{a}_r,\tau_r} ||y_r(t) - \mathbf{f}(t,\tau_r)'\mathbf{a}_r||_F^2 \tag{2.8}$$

   the delays τ_r and weights $\mathbf{a}_r$ can be determined. Such optimization is feasible since both the sources and the time delays are assumed to be independent.

The FADA algorithm can solve the source separation problem both with and without constraints. Since the EMG signals were non-negative, we used the algorithm with the application of non-negativity constraints on the source functions as well as on the mixing coefficients

When non-negativity constraints are imposed on the source functions,the algorithm works by directly determining the time-dependent values of $f_u(t)$ while taking into consideration the constraint $f_u(t) \geq 0$ for the discretely sampled values. The scaling or mixing coefficients denoted by a_{ru} can be constrained to be non-negative by the algorithm while solving the least squares problem to estimate the scaling coefficients in Eq. (2.8). By imposing the linear inequality constraint $a_{ru} \geq 0, \forall r, u$, the problem is converted into a non-negative least squares problem to determine the weights a_{ru}.

2.3 Identification of spatiotemporal synergies using the anechoic demixing algorithm

The anechoic demixing algorithm can be used to identify spatiotemporal synergies by applying specific constraints on its parameters. By determining separate sets of basis

functions for every EMG signal (corresponding to a single channel), grouping them into vectors and setting the temporal delays and scaling factors as equal for the components of each of the vectors, the unifying model can be transformed into the spatiotemporal synergy generative model. To identify spatiotemporal synergies, P sources f_p are assigned to each of the DOFs m in the data, thus resulting in $M.P$ source functions for the entire dataset. The three steps listed below are then carried out iteratively until the solutions converge.

1. For every spatiotemporal primitive, its optimal delay given by τ_p^l is found for each of the trials by using a matching pursuit procedure. In this method, the set of time-shifted source functions that best explain the data are iteratively found. One source function or primitive is taken at a time, and the scalar product of that time-shifted primitive is computed with the original data using every possible delay between 0 and $T-1$. The primitive and delay that produce the largest scalar product with the original data are then selected and their contribution is removed from the original data. This procedure is repeated for all of the primitives until all the optimal delays have been found.

2. For each of the trials l, the difference between the original data and the reconstruction produced by the movement primitives is minimized to update the combination coefficients c_p^l. The reconstructions are produced using model (2.1) assuming that the movement primitives f_u and the delays τ_{ru} are known.

3. Using the optimal weights and delays found in the previous steps, the source functions f_u which correspond to the spatiotemporal primitives $w_p(t)$ in model (2.1) are updated, by estimating their Fourier coefficients in the same way as that used by the unconstrained FADA algorithm. The primitives and weights can be constrained to be non-negative as mentioned previously.

2.4 Variance explained measure for synergies

To quantify how closely the reconstruction patterns generated by combining the synergies resemble the actual EMG data, “total variation” is used as a metric of the same by the FADA algorithm. The original EMG series and the reconstructions are both multivariate time-series, and therefore an appropriate measure of the goodness of reconstruction can

be defined by taking a ratio of the two variances as shown in the equation below. Total variation is simply the trace of the covariance of the activations of muscles, which is used to define a multivariate measure R^2 in the following manner:

$$R^2 = 1 - \frac{\sum_{l=1}^{L} ||\mathbf{X}^l - \mathbf{X}^l_{rec}||}{\sum_{l=1}^{L} ||\mathbf{X}^l - \bar{\mathbf{X}}^l||} \tag{2.9}$$

where $\mathbf{X}^l$ represents the data matrix, $\mathbf{X}^l_{rec}$ represents the reconstructed values produced by mixing the synergies and where $\bar{\mathbf{X}}$ is the matrix of the mean values of the data. R^2 is representative of the fraction of the total variance accounted for by the synergy-based reconstruction.

Chapter 3

Materials and Methods

3.1 Pilot Experiment 1

3.1.1 Subject

One left-handed, male, healthy adult (age 39 years, mass 82 kg, height 178 cm) participated in the experiment. The participant, whose personal details are anonymized, did not have any previous history of neuromuscular disease. He gave his informed written consent to participate in the experiment. The experiment received approval from the ethical committee at the University of Stuttgart, where the experiment was conducted.

3.1.2 Experiment design and apparatus

3.1.2.1 Setup for motor task

The experimental setup consisted of a large square (1 m x 1 m) vertical metallic aluminium frame with 3 horizontal bars, at distances 25 cm, 50 cm and 75 cm from the bottom of the frame respectively. On these bars the targets to be grasped were placed by fixing them onto 2 cm cylindrical projections at fixed locations that were 25 cm apart, on the horizontal bars, such that the 9 target blocks formed a 3 x 3 matrix. These targets were rectangular wooden blocks of approximate dimensions 8 cm x 5 cm x 2 cm. The axis of fixation of the blocks was parallel to their thickness (shortest dimension) and they were were oriented such that the 5 cm sides were aligned with the horizontal. This was done to enable the use of a power grip while grasping the blocks. The entire frame was painted black to minimize reflection, which would otherwise have affected the quality of the motion

capture readings. The vertical frame was supported by two solid, metallic base plates. The setup was designed to facilitate sliding of both the blocks on the horizontal bars, as well as the horizontal bars themselves, however, during the course of the experiment their positions were not changed. The frame was elevated by propping it up between two tables placed side by side such that each of the two base plates rested on a table. This elevation enabled the subject to reach all the different target blocks without having to make any major trunk movements to do so (reducing activation of muscles not required for performing the grasping task).

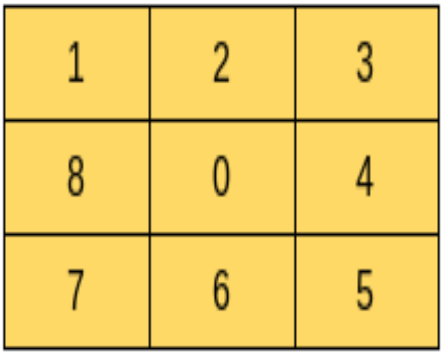

Figure 3.1: Target numbering scheme followed. The grasping of the target blocks, represented by the different numbers, was carried out via directional grasping movements.

3.1.2.2 EMG

3.1.2.2.1 Equipment used:

- Quattrocento OT Bioelectronnica EMG Amplifier
- 3 HD-sEMG 2D arrays of 8 cm x 8 cm, with 64 channels each, from OT Bioelettronica
- 3 EMG pre-amplifiers
- CDE-B 24mm bipolar electrodes with banana connectors
- AUX cable for trigger signal from VICON
- 2 Electrodes used for grounding (at the medial epicondyle and acromion)

3.1.2.2.2 Data Acquisition:

In order to prepare the skin for the measurement of EMG signals, Everi Skin Preparation Gel (Spes Medica, Genova, Italy) was applied to the skin to decrease the epidermal capacitance caused by the lipid content of dead tissue on the skin. It was removed by rubbing alcohol (Kodan Tinktur forte, Schülke & Mayr, Norderstedt, Germany) on the skin. Electro-conductive gel (AC CREAM250V-3, Spes Medica SRL, 16153 Genoa, Italy) was used to increase the conductance of the skin and improve the signal-to-noise ratio of the signals measured.

Muscle activity was recorded from 11 major arm muscles of the subject's right arm (used for the grasping task), using bipolar sEMG electrodes. The muscles whose activity was measured were: 1) Biceps long head 2) Latissimus dorsi 3) Deltoid anterior 4) Deltoid middle 5) Deltoid posterior 6) Trapezius lower 7) Trapezius middle 8) Pectoralis major 9) Sterno cleido occipital mastoides 10) Triceps long head 11) Trapezius upper. The electrodes were positioned appropriately on the muscles such that stretching or bending of electrodes was minimized during movement, in accordance with SENIAM 8 placement recommendations. The electrodes were oriented parallel to the muscle fibres and were placed approximately 20 mm apart. They were fixed to the skin using surgical tape (Fixomull Stretch, BSN Medical GmbH, Hamburg, Germany) and the cables were aligned to form a central branch structure.

HD-EMG signals were recorded from the muscles of the hand (and wrist) by placing the three HD-EMG arrays contiguously around the upper portion of the forearm to form a band. HD-arrays 1, 2 and 3 were placed approximately above the flexor carpi radialis, the flexor carpi ulnaris and the extensor carpi radialis muscles respectively. However, in reality, due to the large number of electrodes and the large size of each HD-array, the signals measured can be considered to be the resultant signal produced by the electrical activity of multiple hand and wrist muscles in proximity to the array.

The EMG signals were sampled by the Quattrocento OT Bioelettronica system at 2048 Hz. The amplification gain for all the bioelectrical signal input channels was 150 V/V. The signals were band-pass filtered (10 - 900 Hz) online. The graphical user interface used to view and monitor the readings online was OTBioLab v 2.064.

3.1.2.3 Kinematics

3.1.2.3.1 Equipment used:

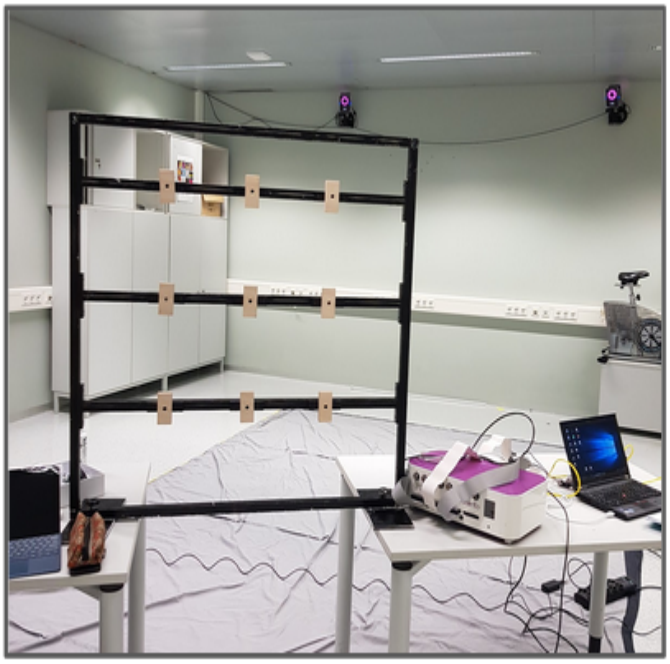

Figure 3.2: Experiment setup: Metal framework with wooden blocks and motion capture cameras are visible. EMG apparatus (purple) is next to the frame, on the right.

- 8 VICON infrared motion capture cameras
- 1 high-speed video camera
- 42 infrared reflector markers

3.1.2.3.2 Data acquisition:

The 8 VICON motion capture cameras were wall mounted on all four walls of the room, facilitating the viewing of the kinematics from different angles. This 360 degree arrangement of the cameras was advantageous because they reduced the probability of occlusion of the markers. The cameras were used to record the three-dimensional trajectory of the grasping motion with the help of the 42 markers, at a sampling rate of 120 Hz. The reflective markers were stuck on the forehead, the upper body, the right arm and the right hand. Two reference markers were placed at the back of the targets 8 and 4. The marker trajectories were viewed online and processed using VICON Nexus 2.8 software.

Figure 3.3: Subject (anonymized) performing the grasping task with the EMG electrodes and motion capture markers attached.

3.1.2.4 Motor Task

The subject was seated on a chair of adjustable height, in front of the frame, in between the two reference markers placed on the frame (on the other side). The positioning was such that the two reference markers and the subject formed an angle of approximately 60°. The designated task was to perform several different directional point-to-point reaching and grasping tasks in the vertical plane. The starting position for the task was a power grip of the central block (target 0) such that it was grasped along its upper and lower edges with the thumb touching the lower edge and the four other fingers placed side by side, curled over the upper edge. From this starting location, the subject then reached and grasped one of the other 8 targets, thus performing a movement in a specific direction away from the centre. The velocity of the grasping movement was regulated by a metronome set to 60bps. The subject grasped each block during the first beat of every bar and then continued to grip it, until the 4 beats of the bar (4 s) had been completed. He then performed the reverse movement, bringing his hand back to grasp the central

target, again within the same 4 s timeframe. This was done until all the different target blocks had been grasped, and the sequence of grasps was initiated as well as ended by grasping the central block. The subject was instructed to reach forward using only his arm and to reduce trunk movement as much as possible.

The protocol followed for recording the signals is described below. Between each of the two steps, counting from 1 to 3 was carried out aloud in synchronization with the metronome, and the next step was begun on the 4th beat of each bar, by issuing the vocal command 'start'.

- The metronome was started (60 bps setting).
- EMG recording was initiated.
- Motion capture recording was started.
- The motor task started.
- The motor task ended.
- Motion capture recording was stopped.
- EMG recording was stopped.

The motion capture system and the EMG amplifying system were synchronised by means of a trigger signal generated by the motion capture system which was received by the EMG amplifying system as an analog input signal.

Five trials of the experiment were conducted, in which the subject performed the motor task involving the power grip described above. Each trial included one centre-out movement and one out-centre movement corresponding to each of the 8 target blocks, resulting in a total of 8 different types of outward movements and the same number of centre-reaching movements. The order of grasping the different targets was randomized across trials to avoid motor learning of the sequence. The number of the target that was to be grasped was said aloud in synchronization with the metronome, following which it was grasped by the subject, and this was repeated for the entire sequence of numbers in each trial. Only the different centre-out movements were used for further analysis.

3.2 Additional data collected

Data were also collected for some modified tasks which are listed below:

- The earlier setup was slightly modified by rotating the target blocks to orient their shorter sides parallel to the vertical axis. Three experiment trials of the centre-out and out-centre movements corresponding to all the different target blocks were conducted, with randomization across trials. The difference between this task and the previous one was that the distance between the fingers and the thumb was effectively reduced when the blocks were grasped.
- A single trial was conducted in which the central block was also used as a target, making the total number of targets 9. These 9 targets were grasped in a random order, without any centre-out or centre-in movements, with each grasping action lasting twice as long (two bars of the metronome) as in the two previous motor tasks.
- Another modification of the experiment was conducted, in which a twisting motion was added to the grasping task. The blocks were oriented such that their longer edges were parallel to the horizontal. The subject reached out, grasped each of the blocks and rotated them clockwise by 90 degrees such that the shorter sides were parallel to the horizontal. This was done in a random order. Following this, the subject reached out and grasped each of the blocks including the central one, again in a random order, and rotated them in the anti-clockwise direction to return them to their original orientations. Thus, this motor task included a twisting motion in addition to the grasping action.

These additional data were not intended to be used for understanding the underlying data structure, as very few trials were conducted for each of the motor tasks. We aimed to obtain some preliminary data that could provide insights into the viability of conducting similar experiments on a larger scale in the future.

3.3 Observations

- The EMG activation waveform patterns corresponding to the same movements showed poor repeatability across the different trials (explained in detail in the Results section).

- Lack of a T-pose static trial made calibration more challenging for the motion capture data.
- The markers of the motion capture data exhibited considerable flickering.This was possibly due to their occlusion by the motion capture cameras and the setup. This data required extensive manual data cleaning, and the flickering also made it difficult to accurately segment the different grasping tasks based on the raw data.
- When the longer sides of the wooden grasping blocks were aligned with the vertical, the grip type executed by the subject was a power grip, based on the height of each block. However, when the shorter sides were aligned vertically, the grasp type was not truly a precision grip because the height of the block was not small enough.

Based on these observations, several changes were incorporated into the design and protocol of the second pilot experiment to obtain better quality data.

3.4 Pilot Experiment 2

3.4.1 Subject

The healthy male subject who had participated in the first pilot experiment took part in this experiment as well.

3.4.2 Experiment design and apparatus

3.4.2.1 Setup for motor task

The same metallic framework was placed in two different orientations - vertical and horizontal - for this study. These two orientations of the frame facilitated the collection of data for the grasping of the target blocks in a vertical plane as well as a horizontal plane. The vertical setup was similar to the one used earlier. However, due to the poor quality of the EMG data in the previous dataset, the grasping task was modified by changing the starting position of the grasping hand (right hand) of the subject. This was done by clamping a wooden slab on the table on the right side of the subject, such that his right hand could comfortably be placed on it, palm downwards. Since the middle block (target 0) was no

longer being used as the starting location, there were 9 total target blocks in this experiment. To reduce the occlusion of the finger markers, 9 long (approximately 10 cm) metal screws were fixed onto the frame, and the target blocks were affixed to these screws. The distance between the blocks and the frame was increased to reduce the occlusion of the blocks from view.

In the horizontal setup, the metal framework was placed horizontally, propped by the two tables, such that the target blocks faced the ceiling. The blocks were not fixed onto long screws in this setup. Due to the large dimensions of the frame, which was in front of the subject, this resulted in the subject needing to bend forward to reach the farthest target blocks, adding some trunk motion to the grasping movement.

Two different types of blocks were used in this experiment - square ones (approximate dimensions: 8 cm x 8 cm x 2 cm) which were grasped with a power grip, and rectangular ones (approximate dimensions: 8 cm x 2 cm x 2 cm) which were grasped with a precision grip. The axis of fixation of the blocks was parallel to their thickness (shortest dimension). The second set of blocks was aligned such that the smaller sides parallel to the vertical axis. The position of the target blocks was kept fixed throughout the experiment, and the numbering scheme was the same as earlier.

3.4.2.2 EMG

3.4.2.2.1 Equipment used:

- Quattrocento OT Bioelectronnica EMG Amplifier
- 3 HD-sEMG 2D arrays of 8 cm x 8 cm, with 64 channels each, from OT Bioelettronica
- 3 EMG pre-amplifiers
- 16 CDE-B 24mm bipolar electrodes with banana connectors
- 2 Electrodes used for grounding (at the medial epicondyle and acromion)

3.4.2.2.2 Data Acquisition:

The skin was prepared for electrode placement in the same manner as in the previous experiment, using Everi Skin Preparation Gel, Kodan Tinktur Forte and AC CREAM250V-3. Regular sEMG data was recorded from 15 major muscles and 1 hand muscle of the subject's right arm (used for the grasping task) using bipolar electrodes. The muscles

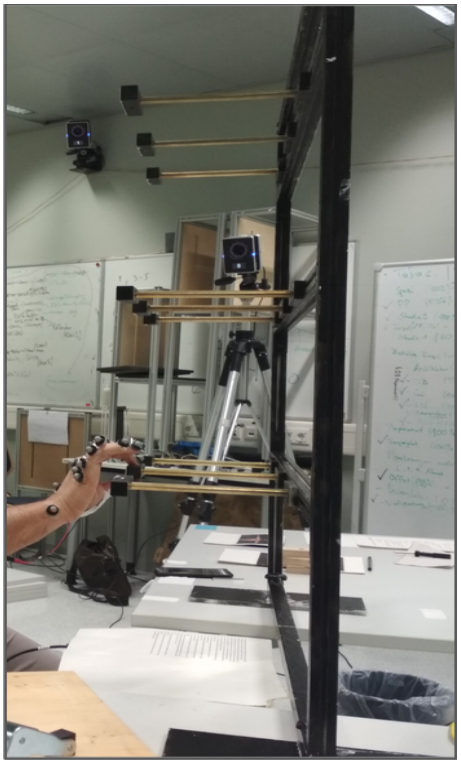

Figure 3.4: Subject performing a grasping task using the vertical setup with the target blocks fixed onto long metal screws.

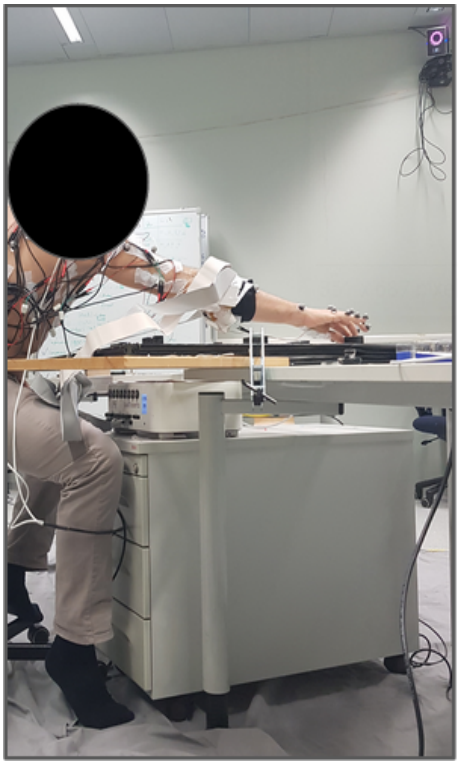

Figure 3.5: Subject performing a grasping task using the horizontal setup.

measured were: 1) Biceps long head 2) Adductor pollicis 3) Latissimus dorsi 4) Anterior deltoid 5) Lateral deltoid 6) Posterior deltoid 7) Lower trapezius 8) Middle trapezius 9) Pectoralis major I 10) Sternocleidomastoid clavicular head 11) Triceps brachii lateral head 12) Triceps brachii medial head 13) Upper trapezius 14) Teres major 15) Infraspinatus 16) Pectoralis major II. Since the Pectoralis major is a large muscle, for this experiment, we decided to make use of two bipolar electrodes to record the electrical activity from two ends of the muscle. The reasoning was that different levels of cross talk would result in different activation patterns across the length of the muscle. Thus, due to its size, this muscle was effectively treated as two different muscles. The electrodes were positioned on the muscles in accordance with SENIAM 8 placement recommendations and fixed using surgical tape. The HD-sEMG signals were recorded in the same manner as in the first experiment, with the three HD-arrays arranged near the the Flexor carpi radialis, the Flexor carpi ulnaris and the Extensor carpi radialis muscles. In this experiment, one of the

EMG bipolar electrodes was used to measure signals from the Adductor pollicis, a hand muscle.

The EMG signals were sampled at 2048 Hz, with an amplification gain of 150 V/V. The signals were band-pass filtered (10 - 900 Hz) online. The graphical user interface used to view and monitor the readings online was OTBioLab v 2.064.

3.4.2.3 Kinematics

3.4.2.3.1 Equipment:

- 8 VICON infrared motion capture cameras
- 1 high-speed video camera
- 46 infrared reflector markers
- Two tripod stands

3.4.2.3.2 Data acquisition:

In an attempt to reduce the flickering of the markers in the kinematics data, the arrangement of the VICON motion capture cameras was modified. Six cameras were wall-mounted in the same positions as in the previous experiment, two were placed on tripod stands and placed on the left and right sides of the subject. The camera positions were adjusted to minimize flickering of the markers, especially those on the fingers of the right hand based on the data visualized online in the VICON Nexus 2.8 software. The reflective markers were stuck on the head, the upper body, the right arm and the right hand.

3.4.2.4 Motor task

The subject was seated on a chair of adjustable height in front of the centre of the metal frame. As described previously, the starting position was the right hand placed palm down on the wooden slab on the right of the subject. By having two orientations of the frame (vertical and horizontal), two sizes of blocks facilitating two grip types (precision and power grip) and two types of reaching movements (reaching with supination and reaching without supination) towards the target blocks, we collected 6 different types of data, each type corresponding to a particular combination of the frame orientation, grip type and reaching movement type. The different types of grasping data collected are listed below:

- Grasp 1: Power grip without supination, using a vertical frame.
- Grasp 2: Power grip with supination, using a vertical frame.
- Grasp 3: Power grip without supination, using a horizontal frame.
- Grasp 4: Precision grip without supination, using a horizontal frame.
- Grasp 5: Precision grip without supination, using a vertical frame.
- Grasp 6: Precision grip with supination, using a vertical frame.

In the horizontal frame setup, the grasping movements did not include supination because it made the movements unnatural and unlike those carried out in everyday life. The protocol followed in the previous pilot experiment was repeated - the target blocks were grasped in a random order, and the subject returned to the starting position after each grasping movement. Movement velocity was regulated using a metronome set to 60 bps.

For each of the 6 types of data, the subject performed 5 experimental trials. In each trial, he grasped all the target blocks in a randomized, orally dictated sequence. The subject was instructed to minimize trunk movements.

The signals were recorded according to the protocol below. Every step was started on the fourth beat of each bar of the metronome.

- The metronome was played aloud at 60 bps.
- EMG recording was started, and due to the synchronization of the two systems, motion capture recording also started simultaneously.
- The motor task started.
- The motor task ended.
- EMG recording was stopped and motion capture recording ceased simultaneously.

The motion capture system and the EMG amplifying system were completely synchronized such that recording from the EMG system automatically resulted in the activation of the motion capture recording system.

3.5 EMG signal processing and analysis

For EMG signals to be used to control biorobotic devices, they need to be extensively processed to remove noise. While measuring any biopotential signal, including EMG, noise may be introduced during the acquisition of analog signals. Thus, extensive digital processing and filtering is a necessity after obtaining the raw data. A Windows 10 OS was used for the offline analysis of the EMG signals. Programs used for signal processing and analysis were written in MATLAB (versions R2016 and R2020a). Plots were generated in MATLAB.

3.5.1 Digital band-pass filtering (20 - 450Hz)

A high-pass filter in series with a low-pass filter together constitute a band-pass filter. Band-pass filtering is used to discard low and high frequency components of the signal, since most of the information contained in the signal is captured by frequencies lying in between the low and high frequency limits. Considering the particular grasping task that we were investigating, we retained signals in the frequency range 20Hz - 450Hz, while the rest were removed by the band-pass filter. A fourth-order butterworth filter (MATLAB “butter” and “filtfilt” functions) was used to to band-pass filter the data.

3.5.2 Removal of Power-Line Interference (Band-stop filter, 50Hz)

One of the types of artifacts affecting EMG recordings is noise introduced due to power-line interference caused by the surrounding electrical network. In Germany, where the data were collected, the standard frequency of the power line is 50Hz. To remove power-line interference, a band-stop filter was used. A band-stop or band rejection filter allows most frequencies to pass without altering them, but selectively removes or attenuates frequencies within a particular range to extremely low levels. Its action is opposite to that of a band-pass filter. A second-order butterworth filter (MATLAB “butter” and “filtfilt” functions) was used to stop the band between 49 and 51 Hz.

3.5.3 Rectification

Rectification is a step carried out prior to other processes, such as envelope extraction. There are two kinds of rectification of digital signals - full-wave rectification and half-wave

rectification. The computation of the absolute value of the raw signals is known as full-wave rectification, whereas passing only the positive values of a signal while setting the negative values to zero is known as half-wave rectification. Full-wave rectification passes twice as many pulses as those allowed through upon half-wave rectification, thus, it is usually considered more suitable for EMG signal processing, and was used by us.

The mean value of the original EMG signals is usually zero or near zero. Upon full-wave rectification, however, the signal is completely positive and its average value fluctuates in tune with the strength of the contraction of the muscle. The rectified signal is of limited use on its own but is a useful input for subsequent processes carried out on the signals. These signals can be used to semi-quantitatively assess the phasic activity and functioning of various muscle groups, as a visual inspection of the changes in amplitude of a signal provides a reasonable indication of the fluctuation in the level of contraction of the muscle concerned.

3.5.4 Low-pass filter (envelope extraction)

A low-pass filter (cutoff 10 Hz) was used to extract the linear envelope. A second-order butterworth filter (MATLAB “butter” and “filtfilt” functions) was used for this purpose. Filtering rectified data with a low-pass filter yields what is known as the linear envelope of the signal. It can be described as a moving average of the signal because it captures the shape of the EMG signal and the trend of the muscle tension curve quite closely. Strong correlations have been observed between the force of muscle contraction and the envelope of the EMG signal during anisotonic isometric contractions.

3.5.5 Segmentation according to kinematics

For the data from the first pilot experiment, the EMG data were segmented such that starting and ending time-points of each of the directional grasping movements (corresponding to the different targets) were determined. 8 directional movements were obtained from the first dataset and 9 directional movements were obtained from the second dataset.

Segmentation was done by hand by visually inspecting the motion capture data in the VICON Nexus software (version 2.9.1). These data were viewed frame by frame and segmented by inspecting the raw data, which were present in the form of the marker trajectories visualized by the cameras. The data were observed from the view of one of the cameras placed on the wall on the right side of the subject, since the hand markers

were placed on the right hand, which was being observed to demarcate the start and end points of the movement. The start point of the movement was denoted by the frame in which the frontal marker on the wrist just started moving. The frame in which all the markers became stationary upon completion of the grasping motion was considered to be the stopping frame of the movement.

There were some issues with the raw kinematics data which could have compromised the accuracy of the segmentation. Many of the markers kept temporarily disappearing, possibly due to temporary occlusion from the view of the cameras. Since the data had not been cleaned at the time of segmentation, the flickering markers made it difficult to accurately determine the end point of the motion. To increase the accuracy of the segmentation, for movements in which the end of the motion was difficult to determine because of flickering, the trajectories were observed from both sides of the hand and the stopping frame number was determined for each side. The higher number was taken to be the stopping frame number for the particular movement being considered.

While recording the first dataset, the start points of the EMG recording and the motion capture recording were not synchronized. The EMG apparatus began recording earlier than the motion capture cameras. The period of synchronization of both types of recordings was stored in the form of an auxiliary signal, a square wave whose start and end points denote the duration (in s) of the motion capture recording, and the corresponding time values in EMG. Thus, the duration of the entire trial can be obtained by subtracting the start point of the square wave from the end point. By obtaining the number of frames in the same trial from VICON, we calculated the frame change rate. The observed frame value was then divided by the frame change rate, which was determined on a trial specific basis, in order to obtain the corresponding time value with respect to the EMG data. The data were segmented and each of the different movements was appropriately labelled according to the movement type (denoted by the target number) for further use. No additional time windows were introduced before the start and end points.

During the second pilot experiment, the EMG and motion capture apparatus recorded synchronously. The 0th second of the EMG recording matched the starting frame in VICON. Thus, the frame change rate per trial was calculated by simply dividing the total number of frames in VICON by the final time value of the EMG readings. To better capture the activity of the muscles from their EMG signals, the time points 200 ms before and after the calculated start and end points were used for the purpose of segmentation. This was done to capture any muscle excitation that occurred prior to the movement as well as any

residual muscle activity after the arm and hand had come to rest.

3.5.6 Time normalization

In order to be able to compare and average signals corresponding to the same movement across the different trials, they were normalized to 90 timepoints using the "interp" function in MATLAB.

3.5.7 Clustering HD-EMG to avoid overrepresentation

HD-sEMG arrays were used to record MEG signals from hand (and wrist) muscles. Three HD arrays were used, each of which had 64 channels, resulting in the use of 192 HD channels in total. The arrays were labelled with the names of the three hand muscles present in close proximity to them - Flexor carpi radialis, Flexor carpi ulnaris and Extensor carpi radialis - but in fact, the signals recorded were produced by a combination of many muscles.

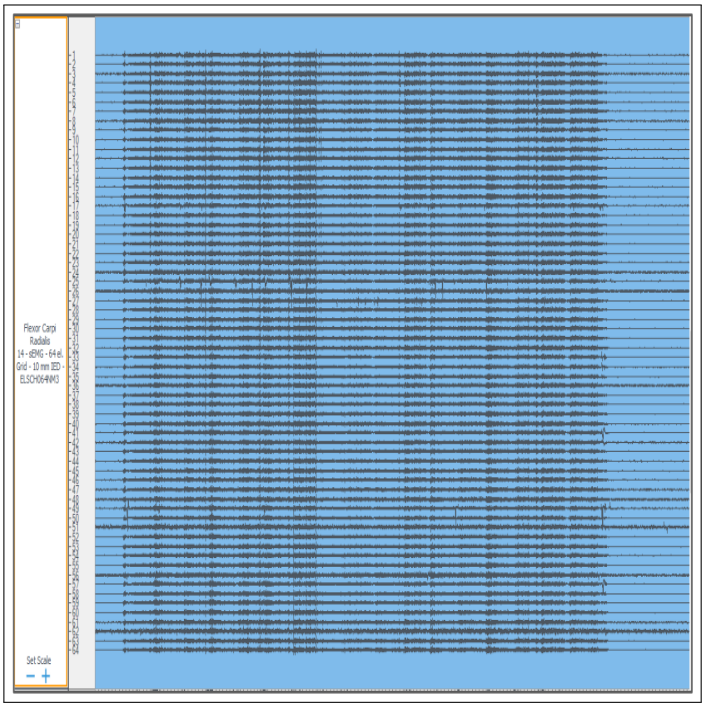

Figure 3.6: 64 correlated HD-sEMG spike trains measured by electrodes present on one of the HD-sEMG arrays. The image displays the amplitude of activation (mV) on the y-axis versus time (s) on the x-axis

It was observed that the temporal activity patterns of signals recorded from a single array were extremely correlated. This was as expected, because the distance between the electrodes on the skin was small and probably not enough to create a large distinction in terms of the particular muscles influencing each of the electrodes. However, having such a large number of correlated channels effectively measuring the activity of the same set of muscles would reduce the accuracy of the synergies extracted from the data. The correlated HD channels, if left unaltered, would vastly outnumber the uncorrelated distinct channels. Given that these channels would be weighted the same as the uncorrelated channels, having so many correlated channels would bias the source separation algorithm. Therefore, we decided to cluster the correlated channels in order to reduce their number.

3.5.7.1 First dataset:

The channels corresponding to a single HD array were reorganised as four square blocks containing 16 channels each. It was observed that there were not many uncorrelated outlier channels within each HD array. The average values of the channels belonging to each of the 4 sub-blocks within an HD array were computed, and the two channels whose values differed most greatly from the mean were discarded. The remaining channels within each sub-block were averaged to produce a surrogate channel representing the sub-block. This resulted in the 192 HD channels being represented by 12 surrogate channels. While averaging, care was taken to strike a balance between having too many channels (at the cost of robustness) and too few channels (loss of information). Using 12 surrogate channels seemed to offer a reasonable balance. However, the 4 channels produced from each array were also fairly correlated.

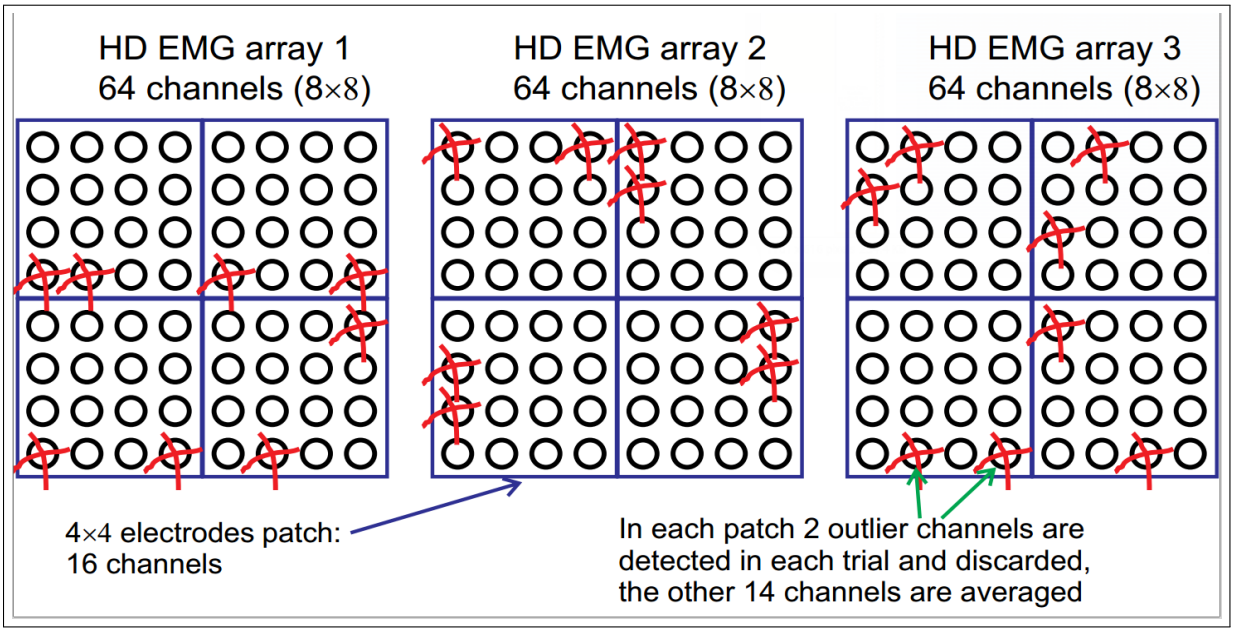

Figure 3.7: The correlated channels of the three HD-sEMG array were clustered by reorganizing the 64 electrodes within each array into 4 equal sized spatial sub-blocks, eliminating outliers and averaging signals within a sub-block (Diagram by Albert M.)

3.5.7.2 Second dataset:

The data were initially clustered using the K-means clustering algorithm. The algorithm is used to divide the data into k clusters such that every data point is assigned to a cluster. At every iteration, the mean of the cluster serves as its representative, and by repeatedly assigning a data point to the cluster whose mean value is nearest to it, similar data points are ultimately grouped together in the same cluster.

Silhouette plots were used to determine the optimal number of clusters per HD-array. These plots provide a measure of the distance between each point present within a cluster and points in the other clusters. If all the points in a cluster have large silhouette values, it indicates that the cluster is well-separated from the others.

These plots confirmed the correlated nature of the channels from each array, and the optimal number of clusters was found to be: 2 for HD-array 1, 1 for HD-array 2 (indicating that all the channels were correlated) and 2 for HD-array 3. This method indicated that the 192 HD channels could be represented by just 5 surrogate channels. However, based on our observations of the data, following this method reduced the number of channels representing the hand by a greater extent than seemed desirable.

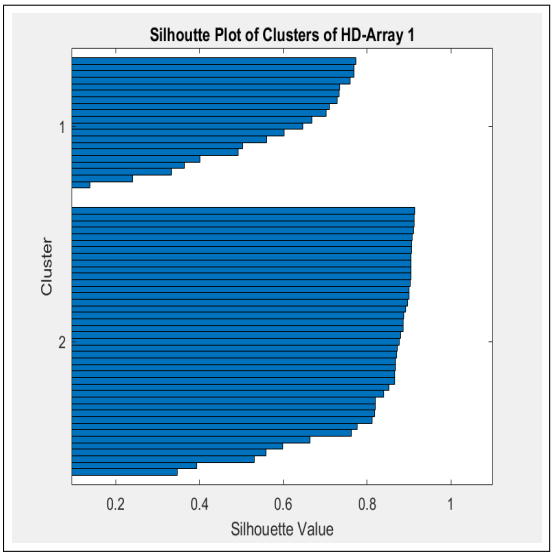

Figure 3.8: The channels of HD-array 1 separated into two clusters. The cluster indices are shown on the y-axis and the x-axis represents the silhouette values of the individual channels.

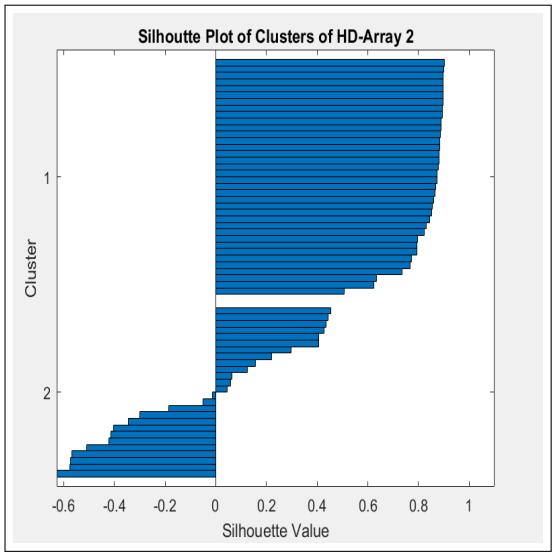

Figure 3.9: The two clusters corresponding to HD-array 2. The cluster indices are shown on the y-axis and the x-axis represents the silhouette values of the individual channels.

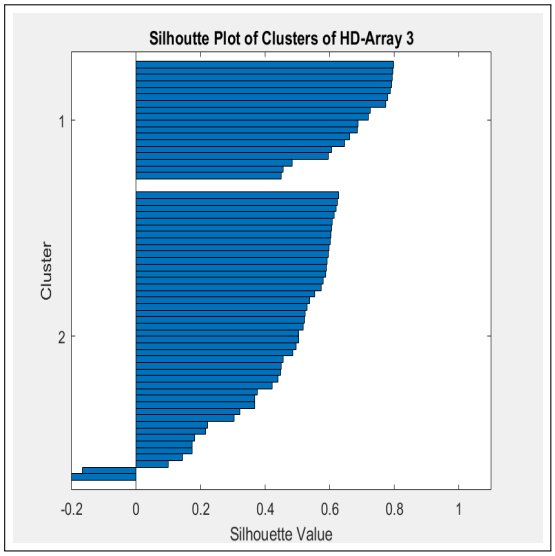

Figure 3.10: The channels of HD-array 3 separated into two clusters. The cluster indices are shown on the y-axis and the x-axis represents the silhouette values of the individual channels.

As visible from the plots, the average silhouette values of the clusters in HD-arrays 1 and 3 are quite high, whereas the average silhouette value of cluster 2 from HD-array

2 is low. This indicates that arrays 1 and 3 can be separated into two distinct clusters, whereas the channels in array 2 cannot be divided into two well-separated clusters.

We therefore implemented the same spatial clustering procedure as used earlier. Prior to the sub-block channels averaging step, a few channels which showed initial activity and no subsequent activity were discarded from the data sub-blocks.

3.5.8 FADA based synergy extraction

Based on the plots of the EMG data, trial 2 was eliminated from the analysis because it did not correspond well with the other trials. Channels 9 and 10 were also excluded from the analysis because they did not show EMG activation waveforms for any of the different directional movements (for all the six grasp types). The data corresponding to the directional movements were horizontally concatenated and the data from the remaining trials were averaged for synergy extraction. Using the FADA toolbox (Chiovetto et al., 2016), spatiotemporal synergies were extracted from the data. 25 harmonics were used. Based on the nature and preprocessing of the EMG data, non-negativity constraints were applied to the synergies, mixing weights and delays. The data had previously been time-normalized to 90 time points per directional movement. To determine the optimum number of synergies to be extracted, the data were categorized into three groups:

- Group 1: All the regular sEMG channels
- Group 2: The surrogate channels from the HD-arrays
- Group 3: A combination of all the regular sEMG and surrogate HD-EMG channels

The first and second groups were considered to be approximately representative of the arm muscles and the hand muscles respectively. Sets of 1, 2, 3, 4 and 5 synergies were extracted from each of these groups. The third group represented all the channels measured from the arm and hand muscles. From this group, sets of 1, 2, 3, 4, 5 and 6 synergies were extracted. To reduce the computational time, for the sets of 4, 5 and 6 synergies extracted from the combined channel data, three runs of the algorithm were used for extraction. For the remaining synergy extractions, four runs of the synergy extraction algorithm were implemented.

For each of the sets of synergies extracted, the algorithm yielded a value for the amount of variance explained by the set of optimized output synergies. These values,

represented by R^2, were plotted against the number of synergies extracted for each of the groups. Such plots usually resemble saturating curves that start to flatten as the increase in the number of synergies results in a lower and lower improvement in the amount of variance explained.

Based on these plots (shown in the Results section), the optimum number of synergies to be extracted from each of the groups, to be used for further analysis, was chosen. Prior to the extraction of these synergies, to obtain more accurate hand and arm synergies, data from the regular EMG channel 2, which measured signals from an intrinsic hand muscle (the adductor pollicis) were moved into group 2 to be analyzed along with the surrogate channels from the extrinsic hand muscles. The synergies extracted from this data were used for reconstruction and the synergy similarity analysis. The synergies extracted from group 3, i.e. from a combination of all the EMG channels, will henceforth be referred to as combined-channel synergies.

3.5.9 Data reconstruction from muscle synergies

The synergies extracted from the three groups of data were used to reconstruct the trial averaged data (excluding trial 4) from the three groups. The optimal weights for reconstruction of the data were determined using the "weightsDelayEstimation" function from the FADA toolbox. Using these optimal weights and delays, along with the previously obtained synergies, the trial averaged data of each of the three groups were reconstructed from the corresponding synergies. The reconstruction of averaged trials was favoured over single trial reconstruction because the individual trial data displayed undulations, which would not be well represented by the smooth source functions obtained from FADA. Averaging the trials resulted in smoother EMG waveforms for the different directional movements, which could be better constructed from the synergies. Due to the limited number of trials available for analysis, the same trial averages were used for the extraction of the synergies as well as to test their data reconstruction ability. However, given that we were trying to ascertain whether our high-dimensional data could be reasonably represented in a lower-dimensional space, this was justified, since it was from the low-dimensional representation (synergies) of the data alone that the high-dimensional data was being reconstructed.

3.5.10 Synergy similarity analysis

We quantitatively analyzed the similarity between the arm synergies and the corresponding channels in the combined-channel synergies, as well as between the hand synergies and the corresponding channels in the combined-channel synergies. The two synergies, w1 and w2, each had D rows corresponding to the number of EMG channels and J columns corresponding to the number of timepoints. To obtain the similarity score, the synergies were normalized using the "norm" function in MATLAB and each channel was demeaned.

Following this, for all possible delays $j \in (1-J, J)$ applied to one of the synergies, say w_2, a vector of $D \times J$ elements v_1^j was built by translating the other synergy w_1 by j, truncating each of its rows and finally rearranging the D rows of w_1 into a single column vector. The D rows of w_2 were then rearranged to form a column vector v_2. The similarity score S is defined as the maximum of the scalar products of the two vectors

$$S = \text{max}_{j \in (1-j,J)}(\mathbf{v}_2^T \cdot \mathbf{v}_1^j) \tag{3.1}$$

The value of the similarity score obtained from the above equation lies between 0 and 1. The highest similarity value and the corresponding delay should ideally match the synergies optimally according to their shapes and should provide a 1:1 mapping between the sets of synergies being compared (the arm synergies and the arm channels of combined-channel synergies as well as the hand synergies and the hand channels of combined-channel synergies).

Exclusion of the demeaning step resulted in the optimal delays being found to be nearly zero for all the pairs, indicating that the mean values of the synergies played a strong role in the matching procedure rather than their shapes. Demeaning the entire synergy instead of each of its channels proved to negatively affect the ability to obtain this 1:1 mapping using this scalar product maximization technique. Thus, the demeaning was carried out on a channel-specific basis, which provided the required 1:1 mapping.

3.5.11 Reconstruction of combined channel data using 1 synergy at a time

To attempt to determine which channels were better explained by each of the combined-channel synergies, we used one of the three synergies at a time to reconstruct the data

and analyzed the variance explained per channel. The reconstruction was carried out in the same manner as before. We decided to identify channels for which the variance explained was > 0.5 (i.e error was < 0.5).

Chapter 4

Results

4.1 EMG Data (Pilot Experiment 1)

The EMG data obtained were processed as described in the Materials and Methods section. The data from the different channels were plotted for all the trials. A good quality EMG recording typically has a well defined waveform for each muscle that is active during a motor task. If the same task is repeated, the EMG waveforms of the same muscle obtained from different trials should have a very similar shape, in a good dataset. However, this was not observed. Without having similar waveforms for EMG signals across trials, it is unlikely that accurate insights into the underlying data structure can be obtained.

To check the quality of the data quantitatively, we carried out a simple ANOVA-based test. EMG data were stored in the form of a time-series, with 90 timepoints. The data for each of the trials were divided into 10 time bins, each with 9 timepoints. The values within a bin were averaged for each of the trials. Thus, each of the 10 time bins contained 5 average values, each pertaining to a different trial. These 5 values were considered as the 'population' for each bin, and a one-way ANOVA test was performed on the means of these populations. The underlying logic was that a defined waveform across trials would produce different mean values in the different time bins, which would show up as significantly different in the ANOVA results.

ANOVA results indicating that the means from the different time bins had been drawn from populations that were not significantly different would point to a lack of a defined EMG waveform across trials. Plots of the data had already indicated that this was the case, and the ANOVA results also confirmed this, by yielding high p-values (> 0.5) for many of the channels for the 8 different directional grasping movements. The insignificant

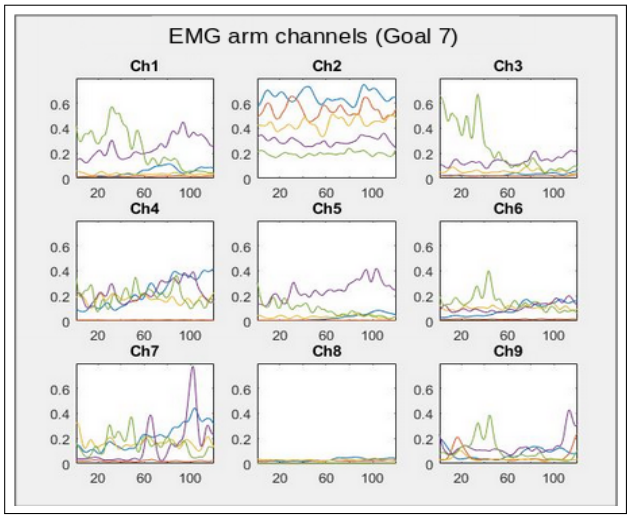

Figure 4.1: Plots of the 9 arm channels from the first set of EMG data,for a particular directional movement (corresponding to target block 7) with each of the trials being represented by a different colour. The y-axis of the subplots represents the amplitude of the signal and the x-axis represents time (normalized)

p-value for a particular channel and a specific grasping movement, could point to either of two cases:

- The data waveform does not show much repeatability across trials, indicating a possibly low signal-to-noise ratio.
- The muscle being recorded by that channel does not contribute to that particular movement, and thus the channel is inactive during the task.

Since not all muscles participate in each of the different types of movements, some of the p-values are expected to be non-significant. However, observing this in all channels or in a large majority of them is indicative of the first case. Since this was what we obtained from our ANOVA analysis, we decided to record new, better quality data for the synergy analysis. The ANOVA test was conducted first on all the five trials and subsequently on the three trials which had better repeatability across channels. Even upon choosing the better trials (trials 1, 3 and 5), a large number of the p-values remained non-significant. The results of the analysis for each of the channels are tabulated below (goals 1 - 8 refer to the different directional movements):

Data for all 5 trials

	Goal 1	Goal 2	Goal 3	Goal 4	Goal 5	Goal 6	Goal 7	Goal 8
Ch 1	0.6791	0.9789	0.9808	0.9980	0.9839	0.9852	0.9998	0.9994
Ch 2	0.9968	0.9853	0.9868	0.9963	0.9725	0.8808	0.9764	0.9824
Ch 3	0.8729	0.9300	0.9178	0.9893	0.9971	0.6543	0.9376	0.9916
Ch 4	0.6806	0.9127	0.9972	0.9954	0.8984	0.9973	0.9997	0.9056
Ch 5	0.5756	0.7880	0.9187	0.9919	0.9888	0.9834	0.9992	0.9594
Ch 6	0.6087	0.4429	0.9886	0.9554	0.9975	0.9981	0.5856	0.4411
Ch 7	0.4349	0.7825	0.6673	0.9987	0.9740	0.9985	0.9997	0.9552
Ch 8	0.2398	0.9993	1.0000	0.9699	0.9361	1.0000	0.9999	0.9600
Ch 9	0.7364	0.9529	0.9884	0.9915	1.0000	0.9865	0.9983	0.8615
Ch 10	0.9030	0.9719	0.9954	0.9470	0.9997	0.9870	0.9578	0.1954
Ch 11	0.9615	0.9568	0.9970	0.9880	0.9996	0.9916	0.9725	0.1152
Ch 12	0.9746	0.9631	0.9978	0.9758	0.9993	0.9674	0.9932	0.2601
Ch 13	0.9875	0.9397	0.9976	0.9899	0.9999	0.9745	0.9649	0.1512
Ch 14	0.9997	0.9739	0.9973	0.9883	1.0000	0.7270	0.9648	0.7418
Ch 15	0.9962	0.9699	0.9986	0.9635	0.9982	0.9430	0.9874	0.4793
Ch 16	0.9994	0.9046	0.9985	0.9984	0.9998	0.9986	0.9914	0.9682
Ch 17	0.9967	0.9805	0.9993	0.9905	0.9993	0.9523	1.0000	0.2115
Ch 18	0.9938	0.9971	0.9780	0.9542	0.9930	0.8216	0.9564	0.7985
Ch 19	0.9994	0.9955	0.9881	0.9862	0.9868	0.9294	0.9835	0.9693
Ch 20	0.9993	0.9987	0.9975	0.9513	0.9752	0.8950	0.9841	0.7743
Ch 21	0.9999	0.9949	0.9896	0.9867	0.9784	0.8867	0.9459	0.9169

Figure 4.2: ANOVA Data for all 5 trials. Red indicates $0 < p < 0.5$, blue indicates $0.5 < p < 0.8$ and black indicates $p > 0.8$

Our data did not strictly satisfy two of the assumptions of the ANOVA statistical test. The first assumption was that of the independence of the different populations being compared, which is not satisfied by time series data. The second assumption was the assumption of normality of the samples in the populations. However, for our purpose, which was to simply get a quantitative confirmation of the lack of a defined EMG waveform across trials, the use of an ANOVA test was appropriate. The results were checked by closely inspecting the data for the few channels that had produced significant p-values. The raw data corresponding to such channels were in agreement with the ANOVA results, as the trials showed greater similarity and a well defined EMG waveform. This validated the use

Data for 3 selected trials (Trials 1, 3 and 5)

	Goal 1	Goal 2	Goal 3	Goal 4	Goal 5	Goal 6	Goal 7	Goal 8
Ch 1	0.6279	0.9605	0.9785	0.9964	0.9727	0.9314	0.9763	0.9997
Ch 2	0.9993	0.9759	0.9856	0.9920	0.9592	1.0000	0.8782	0.9796
Ch 3	0.6551	0.2336	0.0324	0.8883	0.9420	0.9272	0.7950	0.9618
Ch 4	0.6684	0.8298	0.9418	0.9895	0.8319	0.9672	0.9995	0.9176
Ch 5	0.4093	0.4330	0.9359	0.9585	0.7563	0.9997	0.9948	0.9482
Ch 6	0.4064	0.2005	0.8205	0.9490	0.9804	0.9815	0.9279	0.5135
Ch 7	0.1512	0.6424	0.9264	0.9964	0.9540	0.9996	0.9950	0.9522
Ch 8	0.2082	0.9984	0.9891	0.9571	0.8919	0.9939	0.9589	0.9535
Ch 9	0.8429	0.7167	0.8227	0.7787	0.9819	0.9998	0.9637	0.9284
Ch 10	0.7970	0.7009	0.8884	0.9499	0.9582	0.9764	0.9169	0.0039
Ch 11	0.8967	0.7355	0.9438	0.9612	0.9250	0.9928	0.9864	0.0021
Ch 12	0.9488	0.6612	0.8660	0.9606	0.8119	0.9281	0.9665	0.0209
Ch 13	0.9664	0.6444	0.8435	0.9519	0.8719	0.9769	0.9734	0.0219
Ch 14	0.9997	0.9338	0.6931	0.3910	0.9914	0.8603	0.9667	0.4585
Ch 15	0.9911	0.8281	0.7656	0.9591	0.8223	0.8754	0.8603	0.2209
Ch 16	0.9998	0.9198	0.8912	0.6400	0.9037	0.9083	0.9621	0.3917
Ch 17	0.9939	0.8868	0.8437	0.9177	0.9051	0.8611	0.9985	0.1376
Ch 18	0.9907	0.9817	0.3843	0.9496	0.7060	0.8836	0.8699	0.4230
Ch 19	0.9995	0.9258	0.5441	0.9375	0.3973	0.7678	0.9113	0.6039
Ch 20	0.9975	0.9972	0.7422	0.9248	0.2538	0.8298	0.9294	0.6979
Ch 21	0.9999	0.9866	0.6391	0.8999	0.3227	0.6441	0.8443	0.6824

Figure 4.3: ANOVA Data for 3 selected trials. Red indicates $0 < p < 0.5$, blue indicates $0.5 < p < 0.8$ and black indicates $p > 0.8$

of the ANOVA test as a means of analyzing the quality of the data.

4.2 EMG data (Pilot experiment 2)

The EMG data obtained were processed according to the protocol described in the Materials and Methods section. However, one modification was introduced in the segmentation step - a time window of 0.2 s was added before the start and after the end of each of the directional grasping movements, before segmenting them. This was done in order to cap-

ture any activation of the muscles occurring in preparation for the actual movement, as well as any residual muscular excitation after the task had been completed. The data from the different trials were plotted for each of the channels. In this dataset, the trials showed better repeatability of the EMG waveforms for most of the channels as compared to the previous dataset. Some sample plots of the processed EMG data are shown below:

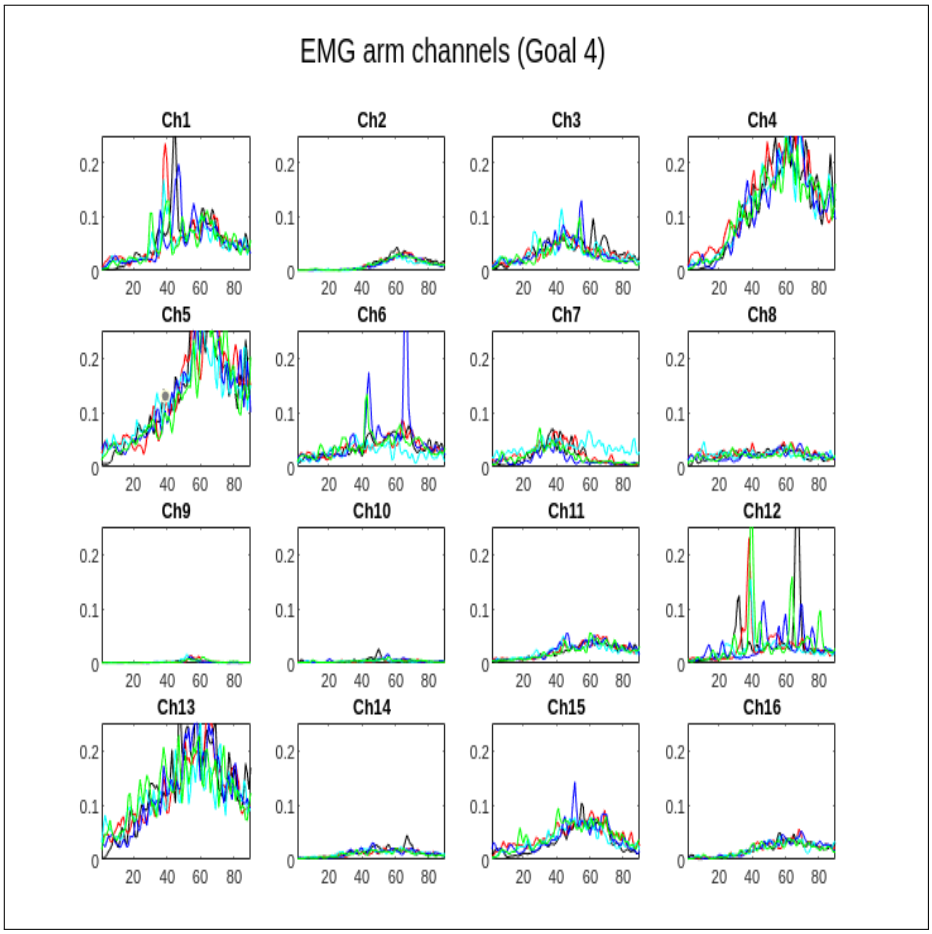

Figure 4.4: Plots of the 16 arm channels from the second set of EMG data, for a particular directional movement (corresponding to target block 4), with each of the trials represented by a different colour. The y-axis of the subplots represents the amplitude of the signal and the x-axis represents time (normalized)

For the purpose of this project, data from the first grasp type (power grip of blocks with the vertical setup and no supination) were used for the synergy analysis. One trial (trial 4) was excluded from the further analysis because the data from this trial did not match the other trials (for most of the channels).

4.3 Plots of explained variance (R^2) vs number of synergies

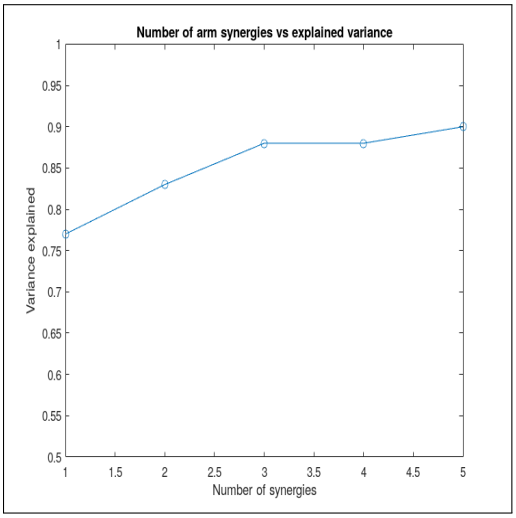

Figure 4.5: Number of synergies versus R^2 for arm channel synergies

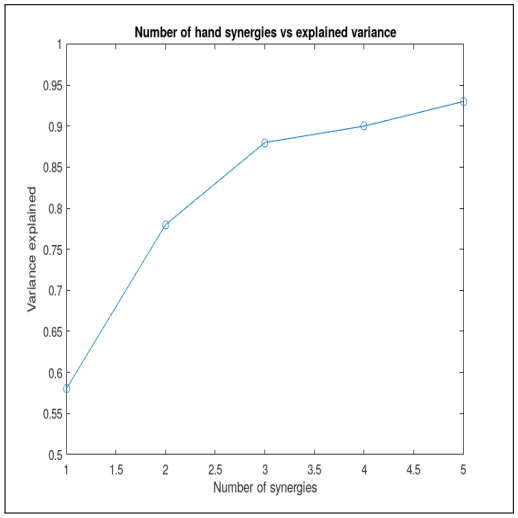

Figure 4.6: Number of synergies versus R^2 for hand channel synergies

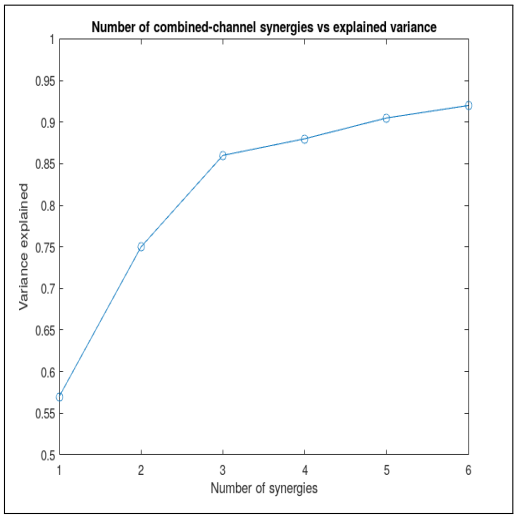

Figure 4.7: Number of synergies versus R^2 for combined-channel synergies

4.4 Synergies extracted from the 3 groups of data

Based on the above plots, 3 was chosen as the optimum number of synergies to be extracted from the different groups for further analysis.

4.4.1 Arm muscle synergies

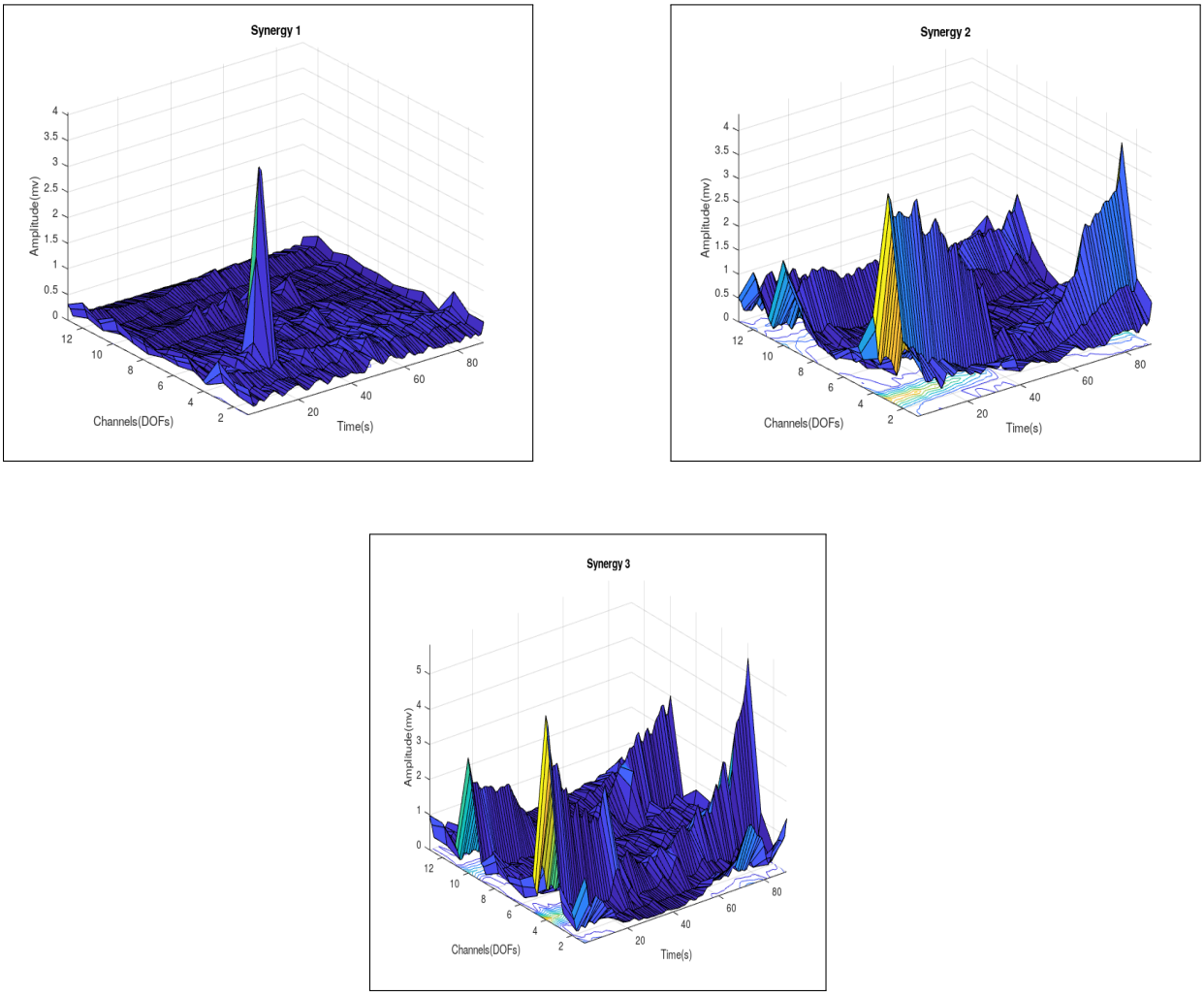

Figure 4.8: Arm muscle synergies

The muscles showing higher levels of activation in each of the arm synergies were:

- Synergy 1: Lateral deltoid

- Synergy 2: Biceps brachii long head, Anterior deltoid, Lateral deltoid, Posterior deltoid, Triceps brachii medial head, Upper trapezius
- Synergy 3: Biceps brachii long head, Latissimus dorsi, Anterior deltoid, lateral deltoid, Triceps brachii medial head, Upper trapezius, Infraspinatus

4.4.2 Hand muscle synergies

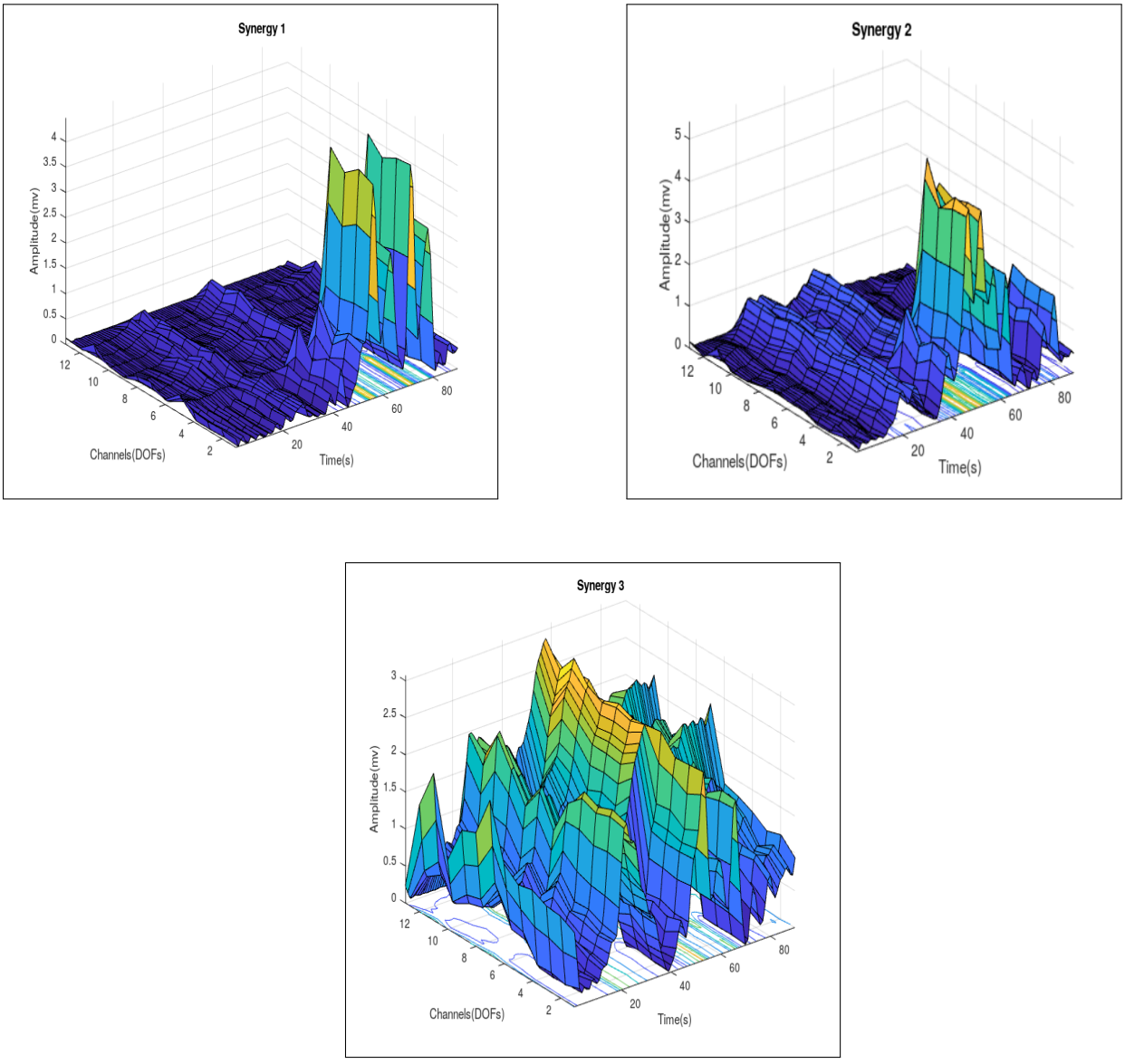

Figure 4.9: Hand muscle synergies

4.4.3 Synergies extracted from the combined arm and hand muscle data

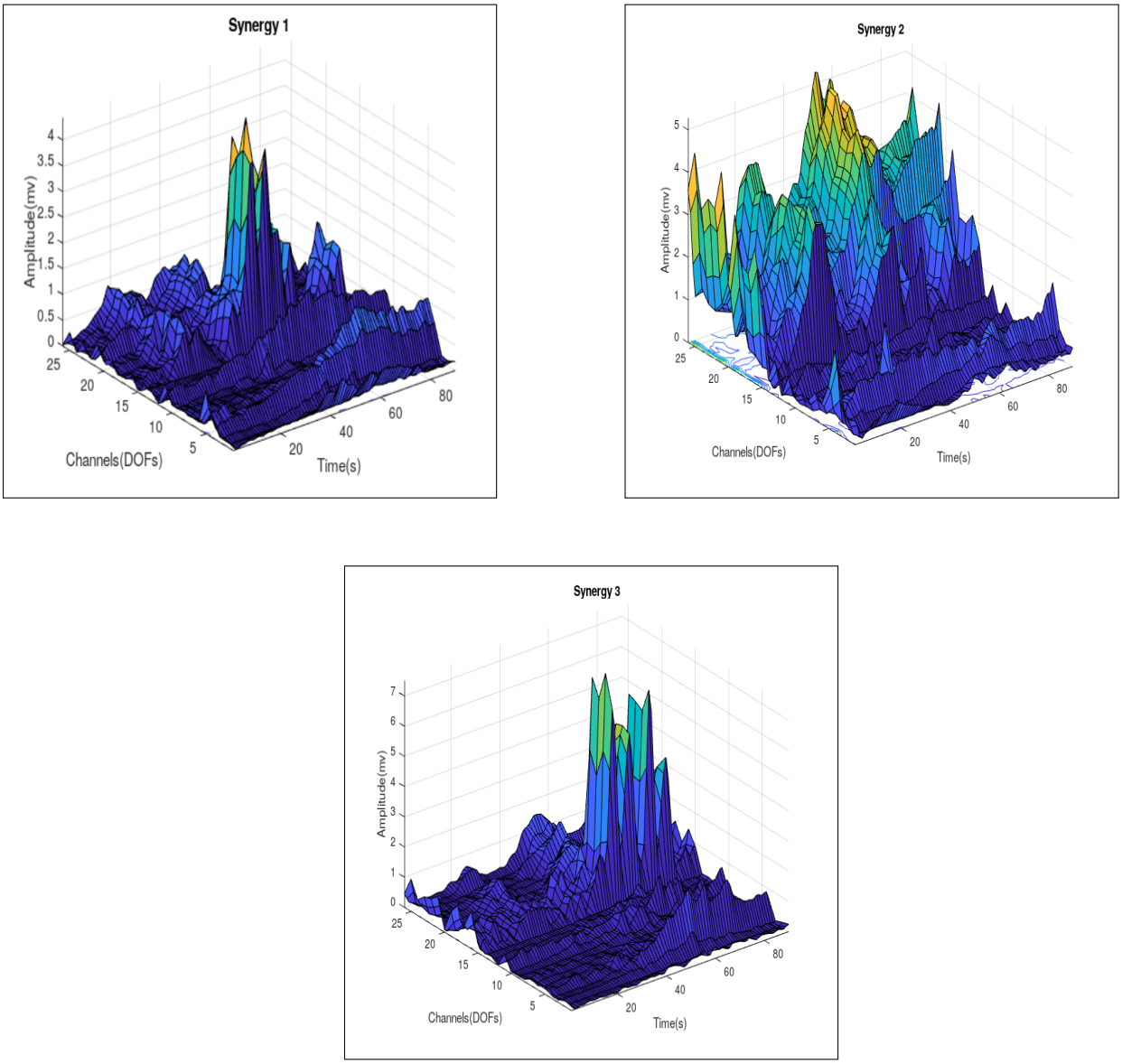

Figure 4.10: Combined-channel synergies

4.5 Data reconstruction from muscle synergies

4.5.1 Reconstruction of arm muscle data from arm synergies

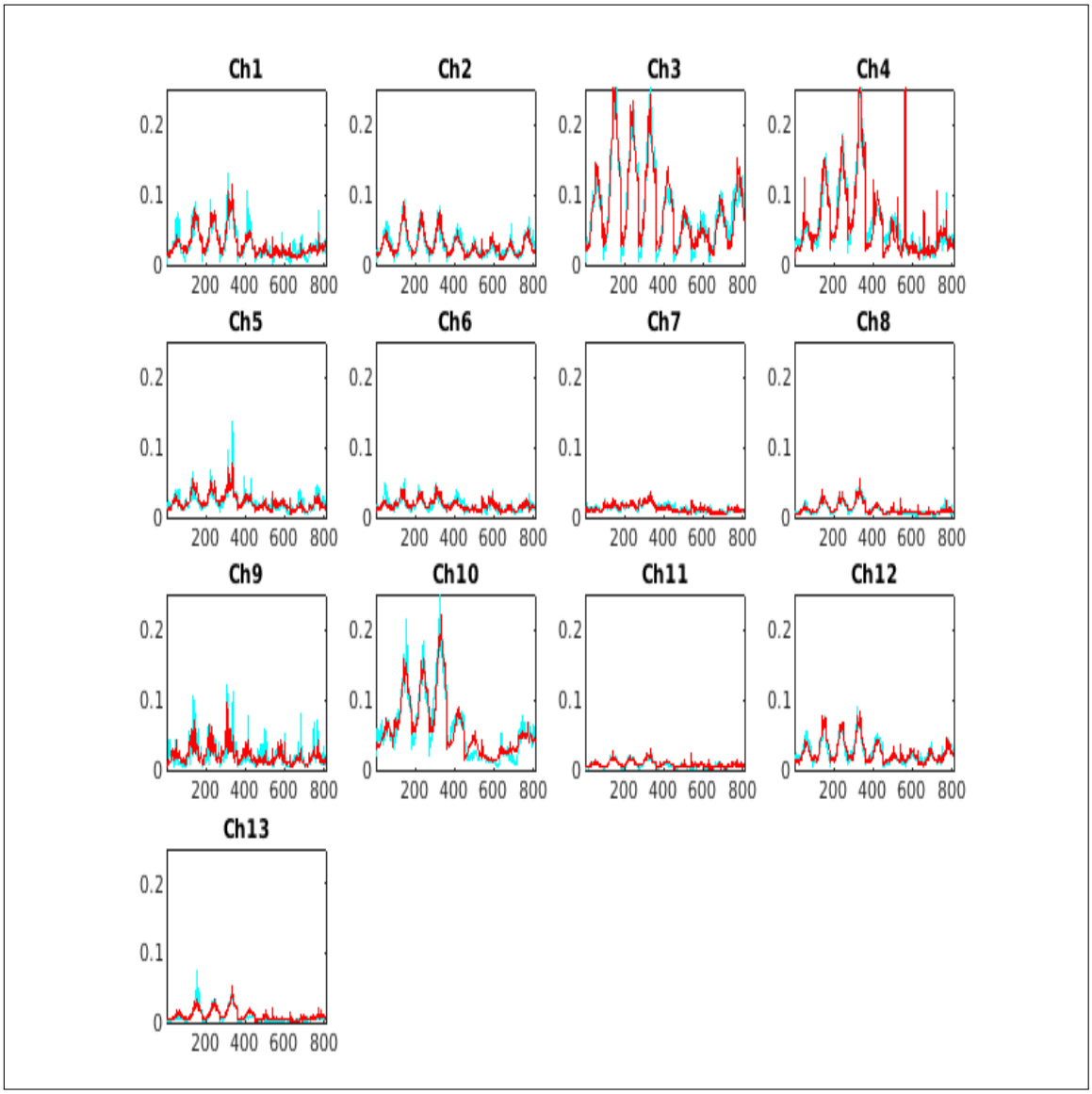

Figure 4.11: Channel-wise reconstruction of the data from all the 9 directional movements (horizontally concatenated) using the three arm synergies. The actual data are represented in blue, and the reconstructions are in red. The y-axis of the subplots represents the amplitude of the signals and the x-axis represents time (normalized)

4.5.2 Reconstruction of hand muscle data from hand synergies

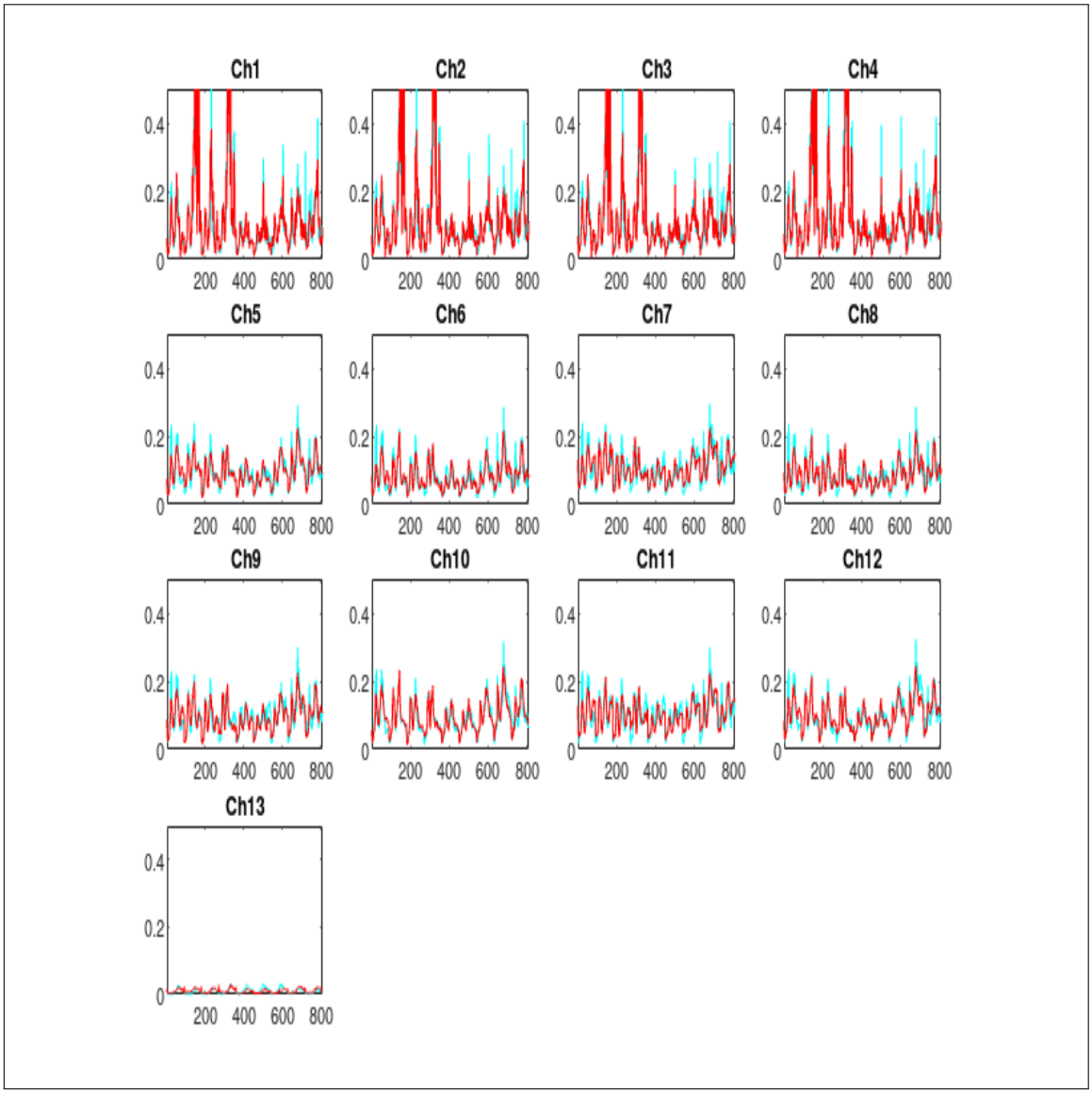

Figure 4.12: Channel-wise reconstruction of the data from all the 9 directional movements (horizontally concatenated) using the three hand synergies. The actual data are represented in blue, and the reconstructions are in red. The y-axis of the subplots represents the amplitude of the signals and the x-axis represents time (normalized)

4.5.3 Reconstruction of data from combined-channel synergies

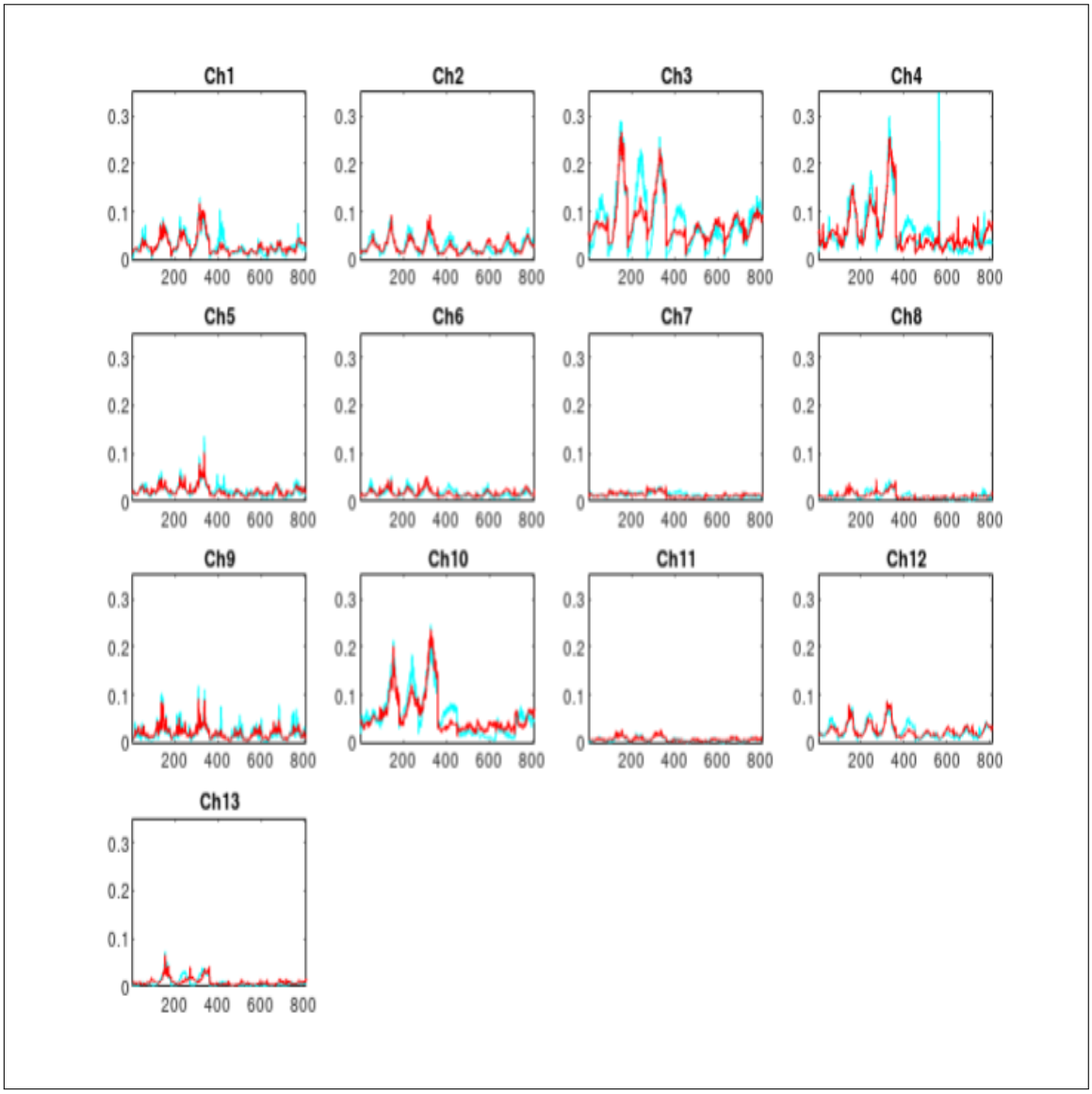

Figure 4.13: Channel-wise reconstruction of the data from all the 9 directional movements (horizontally concatenated) corresponding to the arm channels using the three combined-channel synergies. The actual data are represented in blue, and the reconstructions are in red. The y-axis of the subplots represents the amplitude of the signals and the x-axis represents time (normalized)

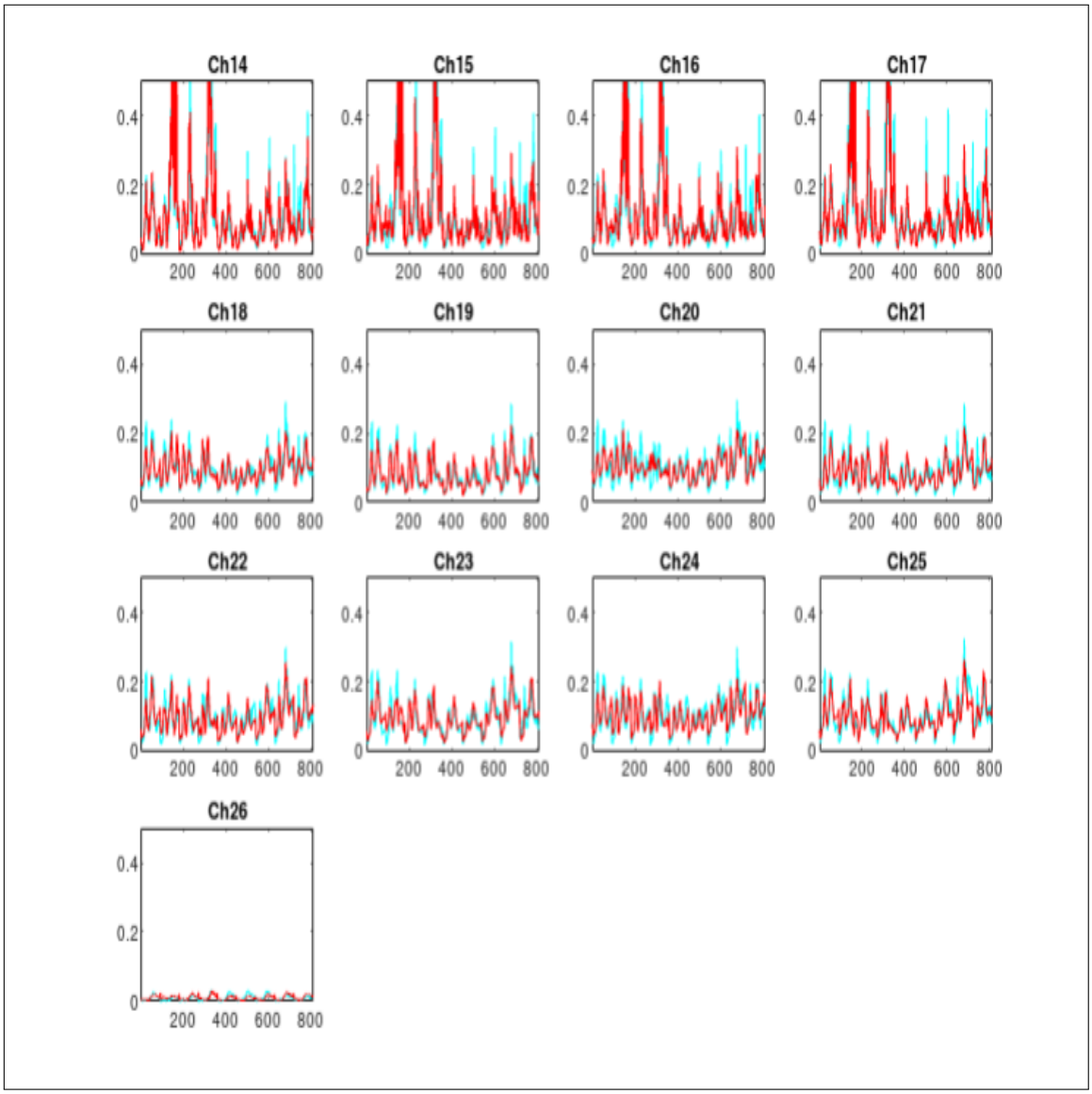

Figure 4.14: Channel-wise reconstruction of the data from all the 9 directional movements (horizontally concatenated) corresponding to the hand channels using the three combined-channel synergies. The actual data are represented in blue, and the reconstructions are in red. The y-axis of the subplots represents the amplitude of the signals and the x-axis represents time (normalized)

The sets of 3 synergies could reconstruct the 9 directional movements quite well, successfully demonstrating that our higher-dimensional EMG data could be reasonably encoded in a lower dimensional space. The R^2 values for all the data reconstructions were > 0.8. The R^2 values of the arm, hand, and combined-channel reconstructions were 0.88, 0.89 and 0.82 respectively.

4.6 Synergy similarity analysis results

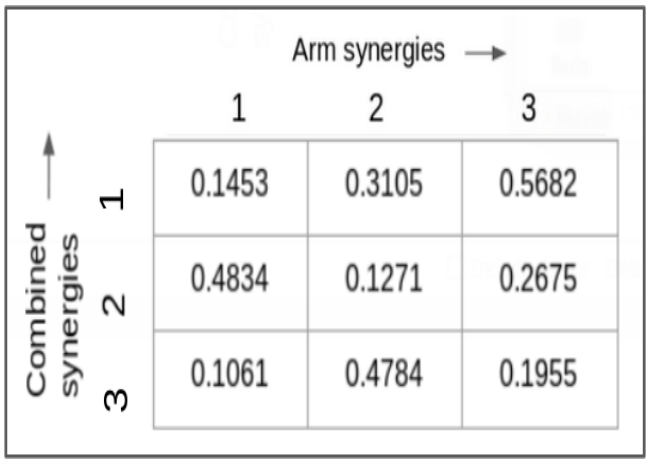

Figure 4.15: The synergy similarity values of the arm synergies and corresponding channels the combined-channel synergies.

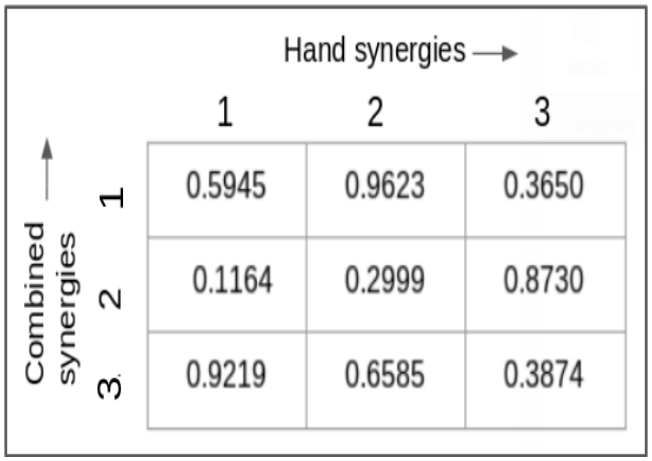

Figure 4.16: The synergy similarity values of the hand synergies and the corresponding channels of the combined-channel synergies.

Using our synergy similarity analysis method, we found 1:1 mappings between the synergies of the arm and hand with the corresponding channels of the combined-channel synergies. A stronger similarity was observed between the synergies of the hand and the corresponding channels in the combined-channel synergies than between the arm synergies and their corresponding channels.

4.7 Reconstruction of combined channel data using 1 synergy at a time

The following results were obtained:

- Reconstruction from synergy 1: Only two arm muscles (anterior deltoid and infraspinatus) had R^2 values > 0.5
- Reconstruction from synergy 2: Only two arm muscles (adductor pollicis and the surrogate hand muscle constituting channel 20) had R^2 values > 0.5.

- Reconstruction from synergy 3: No muscle satisfied the reconstruction threshold when this synergy was used.

Chapter 5

Discussion

With the help of the two pilot experiments, we designed and optimized an experiment design for regular sEMG, HD-sEMG and motion capture data collection. Based on a review of existing motor control papers, we have also developed a robust analysis pipeline for EMG data processing and decomposition. The pilot data obtained, which includes HD-EMG and motion capture data for specific directional grasping tasks with planar targets, can be used to provide valuable insights into the detailed mapping between the EMG activity of the arm muscles and the kinematics of the hand. This mapping, which is crucial for the development of an external exoskeleton device for the hand, is currently being studied by other members of the lab using a synergistic approach as well as an unsupervised Bayesian machine learning approach, based on Gaussian Processes. The unsupervised machine learning approach, which has already yielded some promising results, involves learning the generative model to facilitate the generation of hand kinematics from the EMG data as well as the arm kinematics. A detailed discussion of these approaches is outside the scope of this thesis.

Based on analysis of our pilot data, we have been able to successfully construct the activation patterns of multiple hand and arm muscles from a combination of a few discrete elements. These elements, which are the spatiotemporal synergies obtained by using the FADA algorithm, contain information regarding the underlying spatiotemporal organisation of the muscle activation patterns. The synergies were appropriately scaled and shifted in time to reconstruct the data. They are the common components shared among the different patterns of activation of the muscles, each one representative of a specific level of activation and time-course of the group of muscles being studied.

The representation of data from a high-dimensional space, corresponding to the 9

different directional grasping actions, in a low-dimensional space, using just 3 synergies, is particularly interesting. Based on the plots of explained variance versus the number of synergies, the point at which the elbow curves began to flatten was selected as the optimum number of synergies to be extracted. For all the three cases, 3 was chosen as the optimum number of synergies for extraction. However when only 1 synergy was extracted from the arm channel data, the variance explained value for that synergy from FADA was > 0.75. A close look at the structure of the arm synergies led to the observation that one of the synergies showed significant activation for only one of the muscles (Lateral deltoid muscle). This indicated that the arm muscle data for the 9 directional movements may have been satisfactorily represented by even fewer synergies.

Since the sets of 3 synergies extracted from all the groups were successfully able to explain a large fraction of the variance of the data (> 80 %), this indicates that the data lie in a low-dimensional space, reducing the complexity of the control problem significantly. Research from d'Avella et al., 2003 has shown that there exist similarities between synergies of significantly different behaviours (such as jumping and swimming), weakening the hypothesis that the ability to represent such data in a low dimensional space arises from constraints specific to the task being studied. Consider a reaching movement in a particular direction, corresponding to one of the target blocks in our experimental setup, for example. Due to the redundancy of the musculoskeletal system, various movements may be used to perform the same task, and those movements may be generated by different combinations of muscles. Therefore, a single parameter describing the task could be associated with high-dimensionality due to the potentially large number of muscle patterns associated with it. According to motor control literature, low-dimensionality may be a specific feature of a controller that makes use of a few discrete elements to carry out various different tasks.

Our data are in agreement with the well established line of belief in motor control theory that states that the control of a large number of degrees of freedom is simplified by the CNS with the help of discrete muscle synergies. For our analysis, we obtained muscle synergies from EMG data from the hand and wrist muscles alone, arm muscles alone as well as from the combined data from both hand and wrist muscles. Since there was a difference in the average amplitudes of the regular channels and those from the HD-EMG arrays, with the hand channels displaying higher amplitudes on an average, this possibly resulted in an lower contribution of the Adductor pollicis muscle to the synergies derived from the hand muscles.

Using the similarity metric described previously, we obtained the 1:1 mapping between the synergies from the hand muscles and the corresponding channels of the combined-channel synergies, as well as that between the synergies from the arm muscles and the corresponding channels of the combined-channel synergies. The hand synergies and the combined-channel synergies had higher similarity values. This was possibly due to the fact that despite our spatial clustering of the correlated hand channels, the 12 surrogate channels remained quite correlated, as was inevitable for strongly correlated data such as ours. One possible modification for future analysis could be to reduce the number of surrogate channels from the HD-EMG data or lower the weights of each of the 12 surrogate channels. In our analysis, we opted for the spatial clustering over k-means because it seemed to offer a balance between the loss of information due to dimensional reduction and the bias of the synergy decomposition process because of the correlation of the channels. Based on our results, future analysis of the data can include a further reduction of the number of channels by spatial clustering or by using the few clusters identified by the k-means algorithm.

Our attempt to reconstruct the combined-channel data using only one of the three synergies at a time yielded poor results. This may have been because each of the synergies had the ability to reconstruct some channels better than others, when combined along with the other synergies using appropriate mixing weights. However, when the synergy was used on its own, the weights optimization algorithm may have tried to optimize the weights applied to the synergy with respect to all the channels being constructed. This may have resulted in sub-optimal weights being selected, such that the synergy's reconstruction performance improved for channels it was not reconstructing well when used in combination with other synergies, but not to the extent that the reconstruction threshold was crossed. Similarly, the channels that it was reconstructing well in combination with other synergies, may not have been reconstructed well enough to cross the reconstruction threshold. Overall, due to the sub-optimal weights, the synergy's true channel encoding ability may have been lost. One possible modification of this analysis which could be tried in the future is to zero out multiple groups of randomly clustered muscles in the synergy, calculate the optimal weights (without the influence of the zeroed channels) and reconstruct the data from the synergy, using these weights. The challenging step would be to find out which groups of channels would need to be removed for the estimation of optimal weights.

Other interesting questions can be investigated in the future, using our data. For ex-

ample, the synergies from each of the six grasp paradigms can be extracted and quantitatively compared, to check whether there is an underlying similarity in the representation of fairly different grasp actions. Future work could also try to determine whether there are muscles which have common characteristics or belong to a specific group, which are involved in synergistic coordination during grasping, which would involve modification of the existing synergy analysis pipeline. In addition to this, the tonic activation of the muscles involved in the grasping task could be subtracted from the data and the phasic components alone could be analyzed. In future experiments conducted on a larger scale, additional factors like the addition of different weights to be carried by the subject while grasping could be incorporated.

Bibliography

[1] Alessandro, C., Delis, I., Nori, F., Panzeri, S., Berret, B. (2013). Muscle synergies in neuroscience and robotics: from input-space to task-space perspectives. Frontiers in computational neuroscience, 7, 43.

[2] Caumes, M., de Monsabert, B.G., Hauraix, H., Berton, E., Vigouroux, L. (2019). Complex couplings between joints, muscles and performance: the role of the wrist in grasping. Scientific Reports volume 9, Article number: 19357.

[3] Chiovetto, E., d'Avella, A., Giese, M. (2016). A Unifying Framework for the Identification of Motor Primitives. arXiv:1603.06879.

[4] Chowdhury, R.H., Reaz, M.B.I., Ali, M.A.B.M., Bakar, A.A.A., Chellappan, K., Chang, T.G. (2013). Surface Electromyography Signal Processing and Classification Techniques. Sensors, Vol. 13, pp. 12431-12466.

[5] Cimolato, A. Piovanelli, E., Bortoletto, R., Menegatti, E., Pagello, E. (2016). Muscle synergies for reliable NAO arm motion control: an online simulation with real-time constraints. IEEE International Conference on Simulation, Modeling, and Programming for Autonomous Robots (SIMPAR), San Francisco, CA, USA, pp. 191–196.

[6] d'Avella, A., Portone, A., Fernandez, L., Lacquaniti, F. (2006). Control of fast-reaching movements by muscle synergy combinations. The Journal of neuroscience : the official journal of the Society for Neuroscience, 26(30), pp. 7791–7810.

[7] d'Avella, A., Saltiel, P., Bizzi, E. (2003). Combinations of muscle synergies in the construction of a natural motor behavior. Nature Neuroscience, 6, pp. 300-308.

[8] Drost, G., Stegeman, D.F., van Engelen, B.G.M., Zwarts, M.J. (2006). Clinical applications of high-density surface EMG: A systematic review. Journal of Electromyography and Kinesiology, vol. 16, issue 6, pp. 586-602.

[9] Flash, T. and Hochner, B. (2005). Motor primitives in vertebrates and invertebrates. Current Opinion in Neurobiology, vol. 15, issue 6, pp. 660-666.

[10] Guerra Filho, Gutemberg. (2005). Optical Motion Capture: Theory and Implementation. RITA, 12, pp. 61-90.

[11] Hatem, S. M., Saussez, G., Della Faille, M., Prist, V., Zhang, X., Dispa, D., Bleyenheuft, Y. (2016). Rehabilitation of Motor Function after Stroke: A Multiple Systematic Review Focused on Techniques to Stimulate Upper Extremity Recovery. Frontiers in human neuroscience, 10, pp. 442.

[12] Hermens, H. J., et. al. (1999). SENIAM: European recommendations for surface electromyography : Results of the SENIAM project. Roessingh Research and Development.

[13] Kimura, J. (2001). Electrodiagnosis in Diseases of Nerve and Muscle: Principles and Practice, 3rd Edition. New York, Oxford University Press.

[14] Kuriki, H.U., de Azevedo, F.M., Takahashi, L.S.O., Mello, E.M., Ruben de Faria Negrao Filho, Alves ,N. (2011). The Relationship Between Electromyography and Muscle Force, EMG Methods for Evaluating Muscle and Nerve Function, Mark Schwartz, IntechOpen.

[15] Lacquaniti, F., Soechting, J. F. (1982). Coordination of arm and wrist motion during a reaching task. The Journal of Neuroscience : The official journal of the Society for Neuroscience, 2(4), pp. 399–408.

[16] Ladrova, M., Martinek, R., Nedoma, J., Fajkus, M. (2019). Methods of Power Line Interference Elimination in EMG Signal. Journal of Biomimetics, Biomaterials and Biomedical Engineering, 40, pp. 64–70.

[17] Landsmeer, M.F. (1962). Power grip and precision handling. Ann. Rheum. Dis., 21, 164.

[18] Lunardini, F., Casellato, C., d'Avella, A., Sanger, T.D., Pedrocchi, A. (2016). Robustness and reliability of synergy-based myocontrol of a multiple degree of freedom robotic arm. IEEE Transactions on Neural Systems and Rehabilitation Engineering, vol. 24, no. 9, pp. 940–950.

[19] Marateb, H. R., Farahi, M., Rojas, M., Mañanas, M. A., Farina, D. (2016). Detection of Multiple Innervation Zones from Multi-Channel Surface EMG Recordings with Low Signal-to-Noise Ratio Using Graph-Cut Segmentation. PloS one, 11(12), e0167954.

[20] Mason, C.R., Gomez, J.E., Ebner T.J. (2001). Hand synergies during reach-to-grasp. Journal of Neurophysiology, vol. 89, no. 6.

[21] Mathilde, L., Manelle, M., Etienne, M., Agnès, R.B., Nathanaël, J. (2018). Movement-Based Control for Upper-Limb Prosthetics: Is the Regression Technique the Key to a Robust and Accurate Control? Frontiers in Neurorobotics, Vol. 12.

[22] Nazmi, N., Abdul Rahman, M.A., Yamamoto, S.I., Ahmad, S.A., Zamzuri, H., Mazlan, S.A. (2016). A Review of Classification Techniques of EMG Signals during Isotonic and Isometric Contractions. Sensors vol. 16, 1304.

[23] Raez, M. B., Hussain, M. S., Mohd-Yasin, F. (2006). Techniques of EMG signal analysis: detection, processing, classification and applications. Biological procedures online, 8, pp. 11–35.

[24] Rodríguez, I., Gila-Useros, L., Malanda, A. (2012). Motor Unit Action Potential Duration: Measurement and Significance.

[25] Sarasola-Sanz, A., Irastorza-Landa, N., Shiman, F., Lopez-Larraz, E., Spuler, M., Birbaumer, N., Ramos-Murguialday, A. (2015). EMG-based multi-joint kinematics decoding for robot-aided rehabilitation therapies. IEEE International Conference on Rehabilitation Robotics (ICORR), Singapore, 2015, pp. 229-234.

[26] Scano, A., Dardari, L., Molteni F., Giberti H., Tosatti L.M., d'Avella A. (2019). A Comprehensive Spatial Mapping of Muscle Synergies in Highly Variable Upper-Limb Movements of Healthy Subjects. Frontiers in Physiology Vol. 10.

[27] Singh, R. E., Iqbal, K., White, G., Hutchinson, T. E. (2018). A Systematic Review on Muscle Synergies: From Building Blocks of Motor Behavior to a Neurorehabilitation Tool. Applied bionics and biomechanics, 2018, 3615368.

[28] Türker, K.S. (1993). Electromyography: Some Methodological Problems and Issues, Physical Therapy, Vol. 73, Issue 10, pp. 698–710.

[29] Wikman P.A., Vainio L., Rinne T. (2015). The effect of precision and power grips on activations in human auditory cortex. Frontiers in Neuroscience Vol. 9.

[30] Winter, D.A. (2009). Biomechanics and Motor Control of Human Movement. Wiley.

[31] Winter, D.A., Fuglevand, A.J., Archer, S.E. (1994). Crosstalk in surface electromyography: Theoretical and practical estimates. Journal of Electromyography and Kinesiology, Vol. 4, Issue 1, pp. 15-26.

[32] Zahak Jamal, M. (2012). Signal Acquisition Using Surface EMG and Circuit Design Considerations for Robotic Prosthesis. IntechOpen.